Ma, Y., Cao, T., Snowdon, L., Qian, M., Jiang, Q., Li, M., Mahlstedt, N., Horsfield, B. (2017): Impact of Different Experimental Heating Rates on Calculated Hydrocarbon Generation Kinetics. - *Energy & Fuels*, *31*, 10, pp. 10378—10392.

DOI: http://doi.org/10.1021/acs.energyfuels.7b01035

For submission to: *energy&fuels*

Impact of different experimental heating rates on calculated hydrocarbon generation kinetics

Yuanyuan Ma [1,2], Tingting Cao [1,2], Lloyd Snowdon [1,2], Menhui Qian [1,2], Qigui Jiang [1,2], Maowen Li [1,2]*, Nicolaj Mahlstedt [3], Brian Horsfield [3]

[1]China State Key Laboratory of Shale Oil and Gas Enrichment Mechanisms and Effective Development; [2]SinopecResearch Institute of Petroleum Exploration and Production, 31 Xueyuan Road, Haidian District, Beijing, China, 100083; [3]GFZ German Research Centre for Geosciences, Sektion3.2, Telegrafenberg, 14473 Potsdam, Germany

*Corresponding author (M. Li, E-mail: limw.syky@sinopec.com)

Keywords: pyrolysis; kerogen cracking; optimized kinetics; variable heating rate ranges

Abstract

Four organic rich samples from four basins in China have been analyzed using open system bulk-pyrolysis with heating rates ranging from 0.7 K/min to 40 K/min. The resulting pyrograms have been digitized and first order Arrhenius kinetics optimized using groups of different heating rate ranges. Low heating rate optimization was carried out for data generated at 5 K/min, 2 K/min and either 0.7 K/min or 1 K/min. High heating rate optimization used 15, 25 and 40 K/min experiments. Optimization was also completed for wide heating rate ranges at 40 K/min, 15 K/min and either 1 or 2 K/min. The kinetics solutions were then used to calculate bulk

hydrocarbon generation at a geological heating rate of 3 K/Ma in order to determine the impact of using different experimental approaches.

The results showed that low versus high and narrow versus wide heating rates did not yield systematically different results. The highest predicted geological temperature was observed for the low heating rates (Huadian, Ordos), high heating rates (Maoming) and wide heating rate range (Wang18 and Ordos). The wide heating rate ranges yielded predicted temperatures that were between the high and low heating rates for Huadian and Maoming but higher than or equal to both narrow range rates for Wang18 and Ordos. The results from the Source Rock Analyzer optimized using Kinetics2015 software predicted similar activation energy distributions and frequency factors and consequently similar geological temperatures for all samples to the Rock-Eval results optimized using Kinetics2005 software, although the samples run on the two instruments were not homogeneous aliquots but rather separate pieces broken from field or core samples. Predicted temperatures for 50% transformation at a geological heating rate show a variability of less than $\pm$6 °C, which translates to a burial difference of < 300 m for a basin with a "normal" geothermal gradient.

1. Introduction

The chemical kinetics of kerogen and bitumen cracking have been estimated and used as a critical input to 4D petroleum system models. Conventional petroleum systems [1, 2] encompass a source rock (quantity and type of organic matter), thermal maturation, expulsion (primary migration) plus secondary migration, a suitable reservoir (adequate porosity and permeability) and a trap (effective seal that may have either a structural or stratigraphic configuration). The

timing of the generation/migration and the formation of the trap/seal must be correct. The relative timing is modelled using petroleum generation kinetics. Petroleum systems also must maintain reservoir integrity over geological time to preclude the loss or destruction of the oil or gas product through erosion, seal failure, biodegradation, thermochemical sulfate reduction, and/or other processes.

The initial step in the characterization of compositional petroleum generation kinetics from the selected units was to determine bulk petroleum generation kinetics. This study reports the impact of using different open system analytical hardware (Source Rock Analyzer (SRA) and Rock-Eval 6 (RE6) in different laboratories; GeoForschungsZentrum, Potsdam, Germany and Sinopec Wuxi Institute of Petroleum Geology, China, respectively) at different heating rates (0.7–5 K/min and 1–40 K/min, respectively). Previous studies have investigated the impact of using different heating rates. Schenk and Dieckmann (2004)[3] concluded that the slowest heating rates (0.1, 0.7 and 5 K/min) provided the best kinetics solutions. These authors determined optimized Arrhenius parameters ranging from 1.75×10^{10}/s to 2.85×10^{16}/s with activation energy distribution maxima of 51–63 kcal/mol for a range of samples. In contrast, when Peters et al. (2015)[4] investigated single versus multiple heating rates, they concluded that wide heating rate ranges (including heating rates up to 25 °C/min) provided the best kinetics solutions. Their optimized results showed A values ranging from $2.1 \times 10^{12/}$s (47 kcal/mol) for a Monterey sample to 1.9×10^{16}/s (60.8 kcal/mol) for a Kimmeridge Clay sample depending on which heating rates were used.

In this study, optimized Arrhenius kinetics solutions were determined and compared for four different organic rich samples, two different instruments and a wide range of different

heating rates in order to investigate the impact of different heating rates and different instruments.

2. Samples

Four organic-rich lacustrine shale samples from China were selected for kinetics analysis (Fig. 1). Sample A is a representative of the Huadian oil shale, collected from a fresh opencast mine in the Huadian basin, located within the Dunhua-Mishan fault zone in NE China. It was sampled from the Oil Shale member of Paleogene Huadian Formation [5, 6]. A previous geochemical study [7] demonstrated that the sedimentary provenance of the oil shales was mainly Hercynian and Yanshanian granites as well as andesitic to rhyolitic extrusive rocks, formed in the continental margin orogenic belt belonging to a continental island arc volcanic series. Sample B is an oil shale sample collected from the Eocene to Oligocene Youganguo Formation (E2-3y) in Maoming Basin [8, 9]. It contains up to 80% kaolinite in clay minerals, and was deposited in subtropical-temperate climatic conditions, in a continental rift basin with occasional marine incursions (Zhu, 2007 and references therein)[10]. Sample C is a Lower Paleocene Shahejie Formation (ES4) shale sample, collected from the Wang 18 well (at the depth of 1628 m), Jiyang depression of Bohai Bay Basin [11]. The petroleum geology and geochemistry of the Es4 hydrocarbon source rocks in the study area were discussed previously

Fig. 1. Location of four organic rich samples from China.

by Li et al. (2003) and Pang et al. (2003)[12, 13]. Briefly, this source interval was deposited in a hypersaline, lacustrine setting with TOC contents in the 2–8% range and variable organic matter type. Sample D is an organic rich shale from the Upper Triassic Yanchang Formation (T3C7) in Ordos Basin [14-16], representing fine grained clastic sediments deposited in a large continental depression transformed from a cratonic depression. The ages, sampling locations and stratigraphic information of the samples are listed in Table 1. All samples have a low thermal maturity and are suitable to represent the complete thermal evolution during pyrolysis experiments.

Different portions of the hand specimen samples were selected and prepared separately for the analysis at the GFZ and Wuxi laboratories. There is apparently considerable heterogeneity in the sample material, and thus the samples analyzed in the two laboratories were generally comparable but not identical. For example, the properties of the Oil Shale Member of the Huadian may change rapidly with depth. Sun et al.[5] show TOC contents of 13.1% and 0.1% for adjacent samples only 1 m apart.

3. Methods

Thin sections of the four samples were analyzed using a DM 4500P Leica microscope with software Qwin_V3 for organic petrology, providing visual estimates of the relative abundance of each maceral under reflected and fluorescence inducing light using the area of measured macerals[17]. Relative area percentage is used to represent the relative volume percentage of each maceral.

Aliquots of the four samples were powdered in preparation for pyrolysis analysis. This ensured the homogeneity of the sample material used at the different heating rates within the Wuxi lab. Pyrolysis was performed using a RE6 instrument [18-21] in Wuxi. Sample weights were minimized to avoid as much thermal and diffusion lag as possible. They ranged from ~10.5 mg for the Huadian sample to ~61 mg for the Wang18 sample, with ~38 mg and ~42 mg used for the Maoming and Ordos samples, respectively. These weights are all below the Rock-Eval manufacturer recommended mass of 70 mg per sample. The analysis was performed in two steps: pyrolysis-FID (flame ionization detector) in a nitrogen carrier and oxidation in air using an infrared detector. The initial temperature of pyrolysis was 300 °C, but this temperature was held for 5 min rather than the standard 3 min in order to allow the S1 peak (thermal extraction) to return closer to a baseline before the pyrolysis was initiated. The temperature was then programmed to increase at six different heating rates (1, 2, 5, 15, 25 and 40K/min) to a maximum temperature of 650 °C. The oven was allowed to cool from 650 °C and the FID signal was captured for the first 3 min of the cooling. The pyrolysis experiments were repeated for each sample at 5 K/min and 25 K/min in order to test sampling and instrument reproducibility. The oxidation temperature program was started at 300 °C (1 min hold) and then ramped at 20K/min to 850 °C (5 min hold).

The FID signal was digitized and captured by the RE6 at 1 Hz. The temperature of the thermocouple placed immediately under the sample crucible screen was captured simultaneously and reported as an integer value (°C). There was no dead volume compensation to accommodate the product transfer lag between the sample crucible and the flame ionization detector (FID).

The GFZ aliquots were analyzed by non-isothermal open system pyrolysis at four different laboratory heating rates (0.7 K/min, 2.0 K/min, 5.0 K/min and 15.0 K/min) using an SRA, which also detected the product hydrocarbons with an FID. Kinetic parameters were determined using the three slowest heating rates.

Kinetics 2005 optimization software was used in Wuxi, while a slightly newer version, Kinetics 2015, was used in GFZ to determine the kinetics solutions.

For the RE6 data, the first 5 minutes of the signal were removed (S1 peak) and the time reset to 1 second. The last 3 minutes (180 s) that represents the cool down time of the pyrolysis oven were also removed from the digital file processed in the optimization software. The number of raw data points (collected at 1 Hz) ranged from 525 to 21,000 depending on the heating rate (40 K/min to 1 K/min). The first inflection point (minimum FID signal) was used as the lowest temperature for the pyrolysis data by trimming additional points from the front of the digitized data and the maximum temperature used was selected at the point when the signal returned to a baseline. A linear baseline correction was used to remove any residual S1 signal that extended beyond the initial 5 min hold. The trimmed and baseline corrected data were inspected to ensure that there were no negative FID response values introduced by the correction. The heating rate data were thinned using the Kinetics 2005 software by deleting every second data point sequentially until the pyrolysis curve was represented by 514–856 points and then the temperature was smoothed using a 3 point moving average after which the signal was smoothed, also using a 3 point moving average. Smoothing the temperature data slightly increased the accuracy of that parameter by interpolating one or two additional

155 temperature values between the integer values reported by the RE6. It is important to thin the
156 data before smoothing the temperature to avoid introducing temperature trace artifacts.

157 For each sample, two optimization approaches were used to derive different kinetics
158 solutions. The first method allows a single frequency factor (A) that is applied to all activation
159 energy (Ea) values to be a free parameter that is optimized along with initial potentials (X_i) for
160 each Ea. Up to 25 discrete Ea were allowed with a spacing of 1 kcal/mol (4.184 kJ/mol). In the
161 second optimization procedure, A was fixed to be 3×10^{13}/s (3E+13/s). This approach allows the
162 histograms of X_i as a function of activation energy to be compared directly for different runs
163 and different samples. Only the first method (optimized A) was used at GFZ and thus the X_i
164 histogram distributions cannot be compared directly because of the variability of the A values
165 among the samples.

166 The kinetic models were extrapolated to geological heating rates of 1, 3 and 10 K/Ma.
167 The range of heating rates was used to observe the predicted influence of different geological
168 circumstances. Solutions from the Wuxi lab were compared with the GFZ results using a
169 geological heating rate of 3 K/Ma and the comparison of the different optimization procedures
170 was also made using the geological heating rate of 3K/Ma.

171 In order to compare the initial potential (X_i)-Ea distributions for the different pyrolysis
172 instruments, the Wuxi pyrolysis results were also optimized using a frequency factor that was
173 fixed to be equal to that determined during the GFZ optimization.

174 Solutions with both optimized A and fixed A (3E+13/s) were determined for the Wuxi
175 data using four different groups of heating rates. The first of these used only the three lowest
176 heating rates: 1 K/min, 2 K/min and 5 K/min (group L). This approach was very similar to that

used at GFZ. The second optimization used only the high heating rates: 15 K/min, 25 K/min and 40 K/min (group H). The third set used the widest possible variation in heating rate: 1 K/min, 15 K/min and 40 K/min (group W_1) while a fourth optimization used 2 K/min, 15 K/min and 40K/min (group W_2) in order to get the widest range of heating rate while avoiding the 1 K/min data, which may be susceptible to higher analytical error because of the low absolute FID signal level.

Cumulative petroleum generation curves were calculated using the four bulk kinetic solutions determined in Wuxi (different heating rate groups and optimized A) and the solution obtained at GFZ (using heating rates of 0.7 K/min, 2.0 K/min and 5.0 K/min). The predictions of the different kinetics solutions were compared at a geological heating rate of 3 K/Ma.

4. Results

Photomicrographs of the thin sections of the studied shale samples are shown in Fig. 2. Microscopically, the organic macerals of the Huadian, Maoming and Ordos shale samples consist mainly of algae and minor amounts of vitrinite. In the Huadian sample, 96.2% of algae

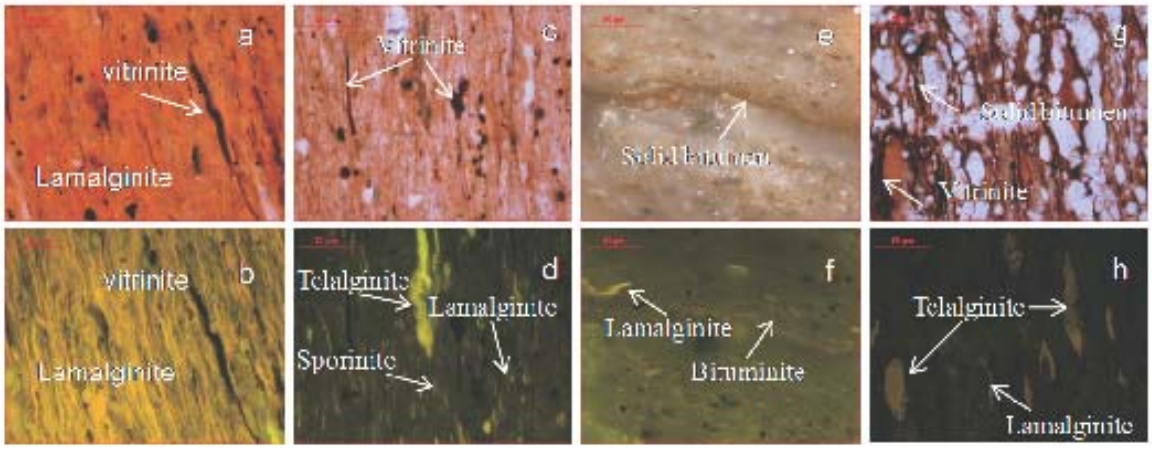

Fig. 2. Photomicrographs of macerals in the four samples (a, c, g: transmitted light; e: reflected white light; b, d, f, h: fluorescene blue light). (a, b:Huadian; c, d: Maoming; e, f: Wang18; g, h: Ordos), polished thin section, immersion oil objective, ×500, scale bar = 50 μm.

192
193 are lamalginite with yellow to orange fluorescence, (Fig. 2b). For the Maoming and Ordos
194 samples, the algae are composed predominantly of lamalginite with yellow fluorescence, and
195 minor telalginite (Fig. 2d, h). While abundant telalginite and minor amount of sporinite occur in
196 the Maoming sample, botryococcus with yellow fluorescence was observed in the Ordos
197 sample (Fig. 2h). In contrast, the Wang18 sample displays abundant lamalginite, bituminite and
198 solid bitumen with orange yellow fluorescence, and minor hydrogen-rich vitrinite.

199 Total organic carbon content and Rock-Eval results from Wuxi and GFZ are listed in
200 Table 2a and 2b, respectively. The absolute analytical errors associated with two instruments
201 were not determined within the context of this project. It was assumed that the instruments
202 were operating within the manufacturer specifications. The samples were run in duplicate in
203 the Wuxi lab to rule out analytical artifacts, as discrepancies between the two labs were

204 significant. Differences are discussed below and can probably be ascribed to sample

205 heterogeneity.

206 Examples of RE6 pyrolysis traces at 15 K/min excluding the S1 peak and the cool down signal are shown in Fig. 3a (sample B-Maoming oil shale), 3c (sample

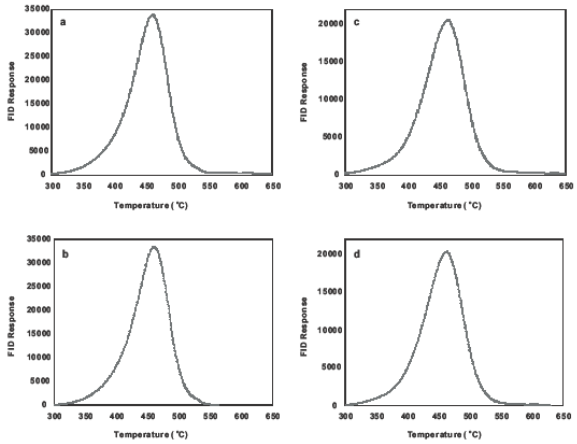

Fig. 3. Examples of RE6 pyrolysis traces at 15 K/min. (a: excluding the S1 peak and the cool down signal for the Maoming sample; b: traces after signal has been trimmed, thinned and the baseline corrected for the Maoming sample; c: excluding the S1 peak and the cool down signal for the Wang18 sample; d: traces after signal has been trimmed, thinned and the baseline corrected for the Wang18 sample).

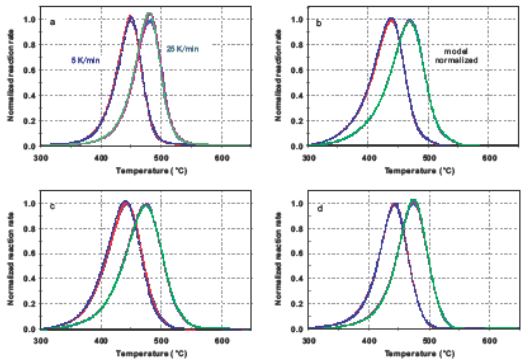

Fig. 4a. A comparison of replicate RE6 runs at 5 K/min and 25 K/min and models calculated with optimized A. (Two sets of measured data and two models are shown for each sample and each heating rate. Traces normalized to the measured data instead of the model. a: Huadian; b: Maoming; c: Wang18; d: Ordos).

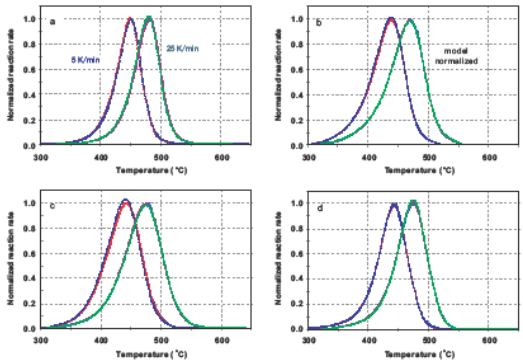

Fig. 4b. A comparison of replicate RE6 runs at 5 K/min and 25 K/min and models calculated with fixed A = 3 × 10^{18}/s. (a: Huadian; b: Maoming; c: Wang18; d: Ordos).

210

211 C-Wang 18 sample). Traces after signals have been trimmed and the baseline corrected for each

212 of the samples are shown in Fig. 3b (sample B-Maoming oil shale), 3d (sample C-Wang 18

213 sample). The input traces for all samples and all heating rates are shown in Appendix A. Fig. 4

displays a comparison of replicate RE6 runs at 5 K/min and 25 K/min. The initial potential (X_i) and activation energy distributions with fixed frequency factor (3×10^{13}/s or 3E+13/s) for group W_1 heating rates for the four samples are illustrated in Fig. 5. The data are listed in Table 3. Histograms for all of the samples and all of the heating rate groups are shown in Appendix B.

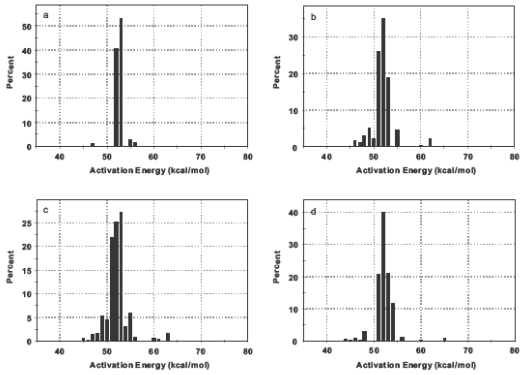

Fig. 5. Initial potential (X_i) histograms for fixed A (3×10^{13}/s) solutions for group W_1 heating rates. (W_1: 1, 15, 40 K/min; a: Huadian; b: Maoming; c: Wang18; d: Ordos).

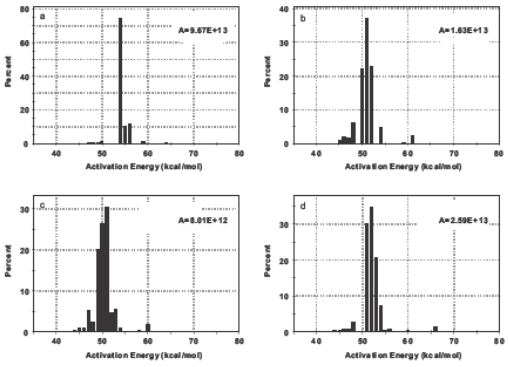

Fig. 6a. Initial potential (X_i) and activation energy distributions calculated for each sample with the frequency factor (A) optimized at group W_1 by Re6.(a: Huadian; b: Maoming; c: Wang18; d: Ordos).

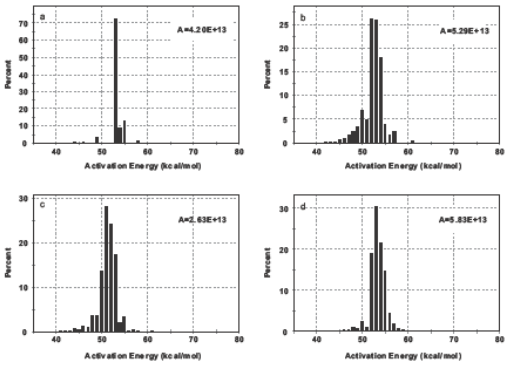

Fig. 6b. Initial potential (X_i) and activation energy distributions calculated for each sample with the frequency factor (A) optimized by SRA. (a: Huadian; b: Maoming; c: Wang18; d: Ordos).

For group W_1 heating rates the initial potential (X_i) and activation energy distributions calculated for each sample with the frequency factor (A) optimized using Wuxi (RE6) data are shown in Fig. 6a, whereas for heating rates of 0.7 K/min, 2.0 K/min and 5.0K/min run on an SRA (GFZ) are shown in Fig. 6b. Histograms for all samples and all heating rates with optimized A are shown in Appendix C. The data are listed in Table 4a-d.

Fig. 7 shows the comparison of the measured data (symbols) and calculated or predicted hydrocarbon yield (curve) for heating rate group W_1. Model fit curves for all of the data are shown in Appendix D.

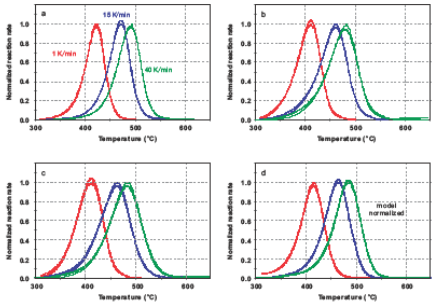

Fig. 7a. Comparison of the measured data (symbols) and calculated or predicted hydrocarbon yield (curve) for heating rate group W_1. (W_1: 1, 15 and 40 K/min; a: Huadian; b: Maoming; c: Wang18; d: Ordos). (with optimized A).

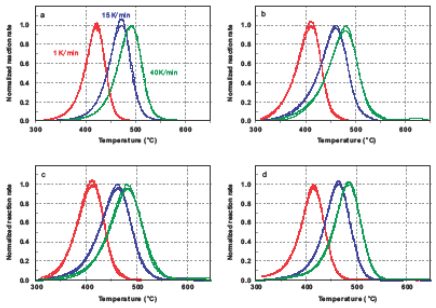

Fig. 7b. Comparison of the measured data (symbols) and calculated or predicted hydrocarbon yield (curve) for heating rate group W_1. (W_1: 1, 15 and 40 K/min; a: Huadian; b: Maoming; c: Wang18; d: Ordos). (with fixed A).

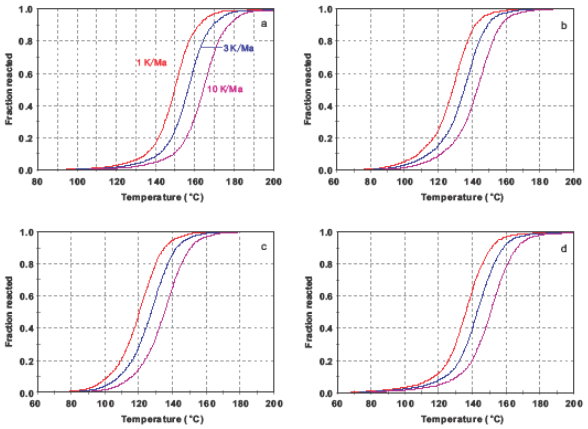

Fig. 8. Comparison of the calculated cumulative HC generation at geological heating rates of 1, 3 and 10 K/Ma for kinetics solutions derived for the low heating rate group L. (L: 1, 2 and 5 K/min) and A optimized for (a) Huadian (b) Maoming (c) Wang18 (d) Ordos

Fig. 8 shows a comparison of the calculated cumulative HC generation at geological heating rates of 1K/Ma, 3 K/Ma and 10 K/Ma for kinetics solutions derived for the low heating rate group (1 K/min, 2 K/min and 5 K/min) and A optimized for (a) Huadian (b) Maoming (c) Wang 18 and (d) Ordos samples. The temperatures for transformation ratios of 10, 30, 50, 70 and 90% are given in Table 5. Fig. 9 displays a comparison of the predicted cumulative hydrocarbon generation at 3 K/Ma for each of the samples and for each of the heating rates groups from the two labs (Table 6).

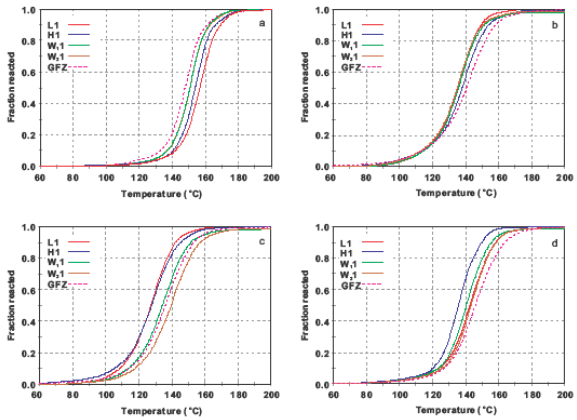

Fig. 9. A comparison of the predicted cumulative hydrocarbon generation at 3 K/Ma for each of the samples and for each of the heating rates groups from the two labs. (L: 1, 2 and 5 K/min; H: 15, 25 and 40 K/min; W_1: 1, 15 and 40 K/min; W_2:2, 15 and 40 K/min and 0.7, 2.0 and 5.0 K/min for GFZ. a: Huadian; b: Maoming; c: Wang18; d: Ordos)

Table 3 lists the initial potential and activation energy distribution for selected Ea categories for a fixed A value (3×10^{13}/s or 3E+13/s) for each of the samples and for each of the heating rate groups along with frequency factors determined for the four samples analyzed using a RE6. Table 4 contains the same solutions but with the optimized A value for each. Table 4 also includes the GFZ solutions and solutions for the Wuxi pyrolysis data optimized with a forced frequency factor equal to that determined by GFZ to allow comparison of SRA and RE6 data. Table 5 lists temperatures (°C) predicted for various TR at a geological heating rate of 1, 3, 10 K/Ma using the kinetics solutions of the low heating rate group (L) and optimized A. Table 6 shows temperatures (°C) predicted for various TR at a geological heating rate of 3 K/Ma using the kinetics solutions of the low, high and wide heating rate ranges and optimized A from Wuxi and compared with GFZ. Fig. 10 shows a comparison of the predicted temperatures for 50% TR at a geological heating rate of 3 K/Ma for the different samples optimized using different heating rate range experiments.

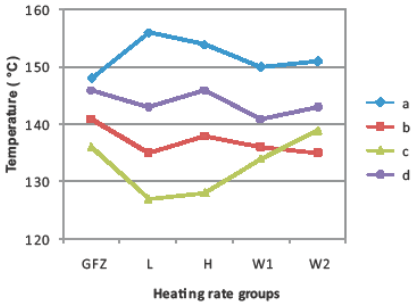

Fig. 10. Temperatures predicted for 50% TR of samples heated at 3 K/Ma as a function of the heating rates used to optimize a kinetics solution. (a: Huadian; b: Maoming; c: Wang18; d: Ordos). Peters et al. (2015) have indicated that solutions Wide1 or Wide2 should provide the best models because these have heating rates that differ by 40× and 20×, respectively. The GFZ-low solution has the lowest heating rate range (0.7–5 K/min) but only a 7.1×ratio. The Low heating rates (Wuxi: 1, 2 and 5 K/min) have a slightly lower ratio of 5, but significantly lower predicted 50% TR temperature for three of the samples.

253 The Arrhenius kinetics parameters (optimized
254 frequency factor and initial potentials for a distribution of activation energies) yielded identical
255 results.

256

257 **5. Discussion**

258 The samples are thermally immature, based on vitrinite reflectance data (Table 2a) and
259 petrographic observations of fluorescence, and generally consistent with Rock-Eval Tmax values
260 between 432–445 °C. (Type I organic matter commonly yields Tmax values of 444±4 °C for all
261 maturities in the initial stage of the oil generation window[22].)

262 The whole rock samples are characterized by high TOC contents ranging from 3.3–32%
263 (Table 2). Wuxi TOC contents of the oil shale samples Huadian, Maoming and Wang 18 are
264 similar to the GFZ data (Table 2b), whereas the TOC content of Ordos sample had a higher TOC
265 content of ~14% instead of 11%. Nevertheless and as previously mentioned, the analytical
266 sample material consisted of sub-samples of pieces of rock and identical results for each
267 sub-sample would be coincidental because the hand specimens were clearly heterogeneous.

S2 ranges from about 16–280 mg/g rock, which is different from the 13–160 mg/g determined by GFZ. Hydrogen Indices (HI) extend from ~330 mg HC/g TOC to ~870 mg HC/g TOC. Thus, the Ordos black mudstone contains Type II/III kerogen (HI < 350 mg HC/g TOC) and samples Maoming and Wang 18 contain Type II kerogen (350 < HI < 600 mg HC/g TOC). The Huadian sample contains Type I kerogen (HI >800 mg/g TOC). The pyrolysis data are consistent with the oil shales which are of lacustrine origin and contain dominantly Type I organic matter, as illustrated by the organic petrology data. The discrepancy in the HI values provided for the Huadian sample between the GFZ and Sinopec labs is puzzling. Fuhrmann et al. [23] have shown for the ES4 member of the lacustrine Shahejie Fm. in the Western Depression of the Liaohe Basin (NE China) that HI values range between 306 and 908 mg HC/g TOC depending on the organofacies within a specific depositional environment (e.g. alkaline shallow lake vs. deep, freshwater lake). This difference was not determined for very closely spaced samples. However, Sun et al.[5] show high contrasts in both TOC (0.1–30.3%) and Hydrogen Index (43–508 mg HC/g TOC) over nine samples spaced at 1 m. The aliquots analyzed in this study were taken within a few centimeters of each other. Perhaps the very high TOC, S2 and HI values represented a thin laminae deposited under euxinic conditions. Clearly, the analysis of additional closely spaced samples would need to be carried out to resolve this discrepancy. Different TOC values or S2 yields would not necessarily affect the kinetics but rather simply the absolute height of the S2 peak. If one aliquot contained more inert organic matter than the other, this will not affect the position (Tmax) or the shape of the S2 peak, but will have an impact on the HI. As long as the reactive organic matter is essentially similar in the two samples, the kinetics solution will be the same.

290 A comparison of replicate RE6 runs at 5 K/min and 25 K/min heating rate (Fig. 4) shows
291 that the raw data curves are virtually superimposable illustrating that the instrument is stable
292 and the data are reproducible. The optimized A and Ea distributions using either of the
293 duplicate runs are essentially identical. That is, the main activation energies were the same with
294 only very small differences noted in the initial potentials.

295 When a fixed frequency factor (A= 3.00E+13/s) is used, the results can be grouped into
296 two general types (Fig. 5, Table 3). Hydrocarbon generation for samples Maoming, Wang 18
297 and Ordos are characterized by a bell-shaped Gaussian-like distribution and for which the
298 activation energy distributions are relatively dispersed. Three main activation energies (51–53
299 kcal/mol) account for ~74% to ~81% of the total bulk reaction. Hydrocarbon generation from
300 the Huadian sample is characterized by a narrower Ea distribution, with two main activation
301 energies accounting for ~93% of the total bulk reaction, indicating a more homogeneous
302 organic matter assemblage.

303 With an optimized A, the Huadian data from both RE6 and SRA are characterized by a
304 narrow Ea distribution in which activation energy ranges over 18 kcal/mol, or 17 kcal/mol for
305 RE6 pyrolysis data optimized with a forced frequency factor equal to that determined using the
306 SRA. The main Ea of 54 kcal/mol (optimized frequency factor = 9.67E+13/s) or 53kcal/mol (using
307 the SRA optimized frequency factor of 4.20E+13/s) for the RE6 data and 53 kcal/mol (optimized
308 frequency factor = 4.20E+13/s) for the SRA results account for ~74%,~81% and ~73% of the
309 total bulk reaction, respectively. The kinetic results show that optimized A value and the
310 dominant Ea values determined using the RE6 are higher than the results from the SRA for the
311 Huadian sample which is different from the other three samples. For example, the calculated

312 Maoming data show three main Ea values (50–52 kcal/mol) accounting for ~82% of the total
313 bulk reaction by RE6 (optimized frequency factor = 1.63E+13/s), which is lower than that of
314 three main Ea (52–54 kcal/mol) accounting for ~70% of the total bulk reaction by SRA
315 (optimized frequency factor = 5.29E+13/s).

316 The kinetic results calculated from the two different instruments (RE6 and SRA) with the
317 same A show that the main Ea distributions are very similar for three samples: Huadian
318 (A=4.20E+13/s, main Ea=53 kcal/mol), Maoming (A=5.29E+13/s, main Ea=52–54 kcal/mol) and
319 Ordos (A= 5.83E+13/s, main Ea= 52–55 kcal/mol). However the main Ea distribution of the
320 Wang 18 sample analyzed using a RE6 is slightly narrower than that of the SRA (RE6: main Ea=
321 51–53 kcal/mol, SRA: main Ea= 50–53 kcal/mol with A=2.63E+13/s). The difference of initial
322 potential of the main activation energy for the total bulk reaction for the four samples between
323 RE6 and SRA is not large, about 5–9%. The RE6 pyrolysis data solution is close to that of SRA
324 when the optimized SRA frequency factor is used with the RE6 data (Fig. 6, Table 4). The
325 consistent results from the two instruments indicate that both machines have well calibrated
326 FID responses and absolute temperature calibrations.

327 Fig. 7 shows the S2 RE6 pyrolysis curves after being thinned, trimmed and smoothed for
328 the heating rates of 1, 15 and 40 K/min along with the behavior predicted by the Kinetics2005
329 solution. Fig. 7a represents a comparison of data and model fit with optimized A for three
330 heating rates (a: Huadian, b: Maoming, c: Wang18, d: Ordos), while Fig. 7b represents a similar
331 comparison of data and model fit with the fixed A of 3E+13/s. The data fit very well with the
332 model both with optimized A and fixed A as expected because of the compensation effect
333 between A and Ea. The results show that the models are consistent with the analytical data,

with the only discrepancies being small errors at the low and high temperature ranges where the hydrocarbon yield is relatively low.

The kinetics solution from the low heating rate group was applied to geological heating rates of 1 K/Ma, 3 K/Ma and 10 K/Ma (Fig. 8). Hydrocarbon generation predicted from the three geological heating rates are different. With increasing geological heating rate, the solution predicted that hydrocarbon generation shifted to higher temperatures for the four samples. The temperatures for selected TR are shown in Table 5. At the high geological heating rate 50% TR is predicted to occur at about 14 °C higher for the Huadian sample and 15 °C higher for the other three samples relative to the lowest geological heating rate (Table 5). Thus for a typical geothermal gradient of about 30 °C/km, about 500 m of additional burial would be required in a rapidly heating basin relative to one with a low geological heating rate.

Comparison of calculated cumulative HC generation at a geological heating rate of 3 K/Ma for solutions using different heating rate groups with optimized A for RE6 and SRA is displayed in Fig. 9 and Table 6. Fig. 10 shows a graphical summary of the temperatures predicted for 50% TR for the four samples based on the 5 different heating rate groups used for the optimization.

For the Huadian sample analyzed using a RE6, wide heating rate range solutions (group W_1 and W_2) are essentially identical. The wide heating rates yield the lowest geological temperature and the low heating rate yields the highest geological temperature (Figs. 9 and 10). The optimized kinetics solution predicts that 50% transformation will occur at 153 $\pm$3 °C depending on which of the heating rate groups is used. The wide heating rate solutions predicted the lowest 50%TR.

For the Maoming sample, the wide heating rate solutions predicted a 50% TR that is between the high and low heating rate solutions (0–1 °C above the solution using the low heating rates and 2–3 °C below the high heating rate solution). The high heating rate solution predicts 138 °C for 50%TR, 3°C higher than the low heating rate and wide heating rate (group W_2) results. The wide heating rate solution temperatures were quite similar to the low heating rate for different TR values (135 °C and 136 °C). This result is somewhat unexpected because at 40 K/min the experimental temperature error could be several degrees and this error should distort both the high heating rate and the wide heating rate optimizations. The higher temperatures for the higher heating rate could be the result of both a thermal lag (the time it takes to actually heat the sample) and the transfer lag (the time required to move the hydrocarbon product from the sample container to the detector). The latter error reflects the change in the measured pyrolysis temperature while the previously generated hydrocarbons move from the crucible to the detector.

For the Wang18 sample, 50% TR is predicted to occur at 133 $\pm$ 6 °C for the different heating rate groups. The wide heating rate solutions (groups $W_1$and W_2) vary by 5 °C, but both predict higher 50%TR temperatures than either the low or high heating rates, unlike the previous two samples. In contrast, the high heating rate yields the lowest geological temperature for the Ordos sample (Table 6). The kinetics solution predicts that 50% TR will occur at 136 °C for the high heating rate, which is 7 °C lower than the low heating rate and wide heating rate group W_2, 5 °C lower than the wide heating rate group W_1. That is, W_1, W_2 and the low heating rate optimizations all provide similar predicted geological temperatures for 50% TR. This is somewhat inconsistent with Peters et al.[4] who indicate that wide heating rate ranges

(three pyrolysis ramps that span at least a 20-fold rate variation) provide the best kinetics solutions in so far as the Ordos results indicate little or no advantage over including only lower heating rates.

Hydrocarbon generation predictions calculated by RE6 are similar to SRA results (Fig. 9 and Table 6). SRA-based extrapolations are closest to those of the high heating rate group for the Maoming sample (Fig. 9b) and closest to those of the wide heating rate group for all other samples. The Huadian sample is 2 °C lower at 50% TR, Wang 18 is 2 °C higher and Ordos is 3 °C higher at 50% TR. The different predicted temperatures for 50% conversion are all within 10 °C for a geological heating rate.

When the frequency factor from the SRA (GFZ) optimization is used with the RE6 (Wuxi) pyrolysis data, the Ea values are similar to those from the SRA (Table 4), even though the samples were not identical. The similarity is inferred to be the result of the similarity in the character of the reactive organic matter, despite small differences in the total amount of TOC in the different sample aliquots. Consequently, the two instruments provide similar predictions for the geological temperatures for the various TR values (Figs. 9 and 10).

The kinetics results calculated using either the Kinetics2005 or Kinetics2015 software is identical for the Maoming sample (Fig. 11) as well as for the other three samples.

6. Conclusions

Two general hydrocarbon generation profiles are observed and modeled for four lacustrine shale samples with both fixed and optimized frequency factors. One is a bell-shaped, Gaussian-like distribution for which the optimized Ea distribution is relatively broad (Maoming,

Wang18 and Ordos samples). The Huadian sample has both a narrower pyrolysis S2 peak and consequently a narrow distribution of optimized activation energies (Ea).

For solutions with an optimized frequency factor, the Ea distribution and A values were slightly higher for the SRA than for the RE6 results, except for the Huadian sample. However, the RE6 solution was close to that of the SRA if the RE6 data were optimized with the frequency factor set to the value determined using the SRA data.

Optimized kinetic solutions derived using different heating rate ranges (1–5 K/min, 15–40 K/min, 1–40 K/min and 2–40 K/min) did not yield systematically different or predictable trends for petroleum generation at geological heating rates. All solutions are essentially similar for the Maoming sample and the differences for the different optimization approaches for the other samples were within a few degrees when modeled at a geological heating rate of 3 K/Ma.

The optimized kinetics solutions from the SRA and Rock-Eval 6 instruments are essentially similar with the SRA results predicting lower temperatures for the Huadian sample, slightly higher temperatures for the Maoming and Ordos samples and temperatures within the distribution for the different RE6 heating rates for the Wang 18 sample. The different solutions for the different instruments and different heating rates would result in different burial depths at maximum thermal stress of about 300 m for a basin with a “normal” geothermal gradient.

Acknowledgments

418 The authors acknowledge the financial support of China Major Science 973 Projects (No.
419 2014CB239101), and Sinopec management for permission to publish this work. We thank Dr.
420 Zhirong Zhang for useful discussion.

421

Figures

Fig. 1. Location of four organic rich samples from China.

Fig. 2. Photomicrographs of macerals in the four samples (a, c, g: transmitted light; e: reflected white light; b, d, f, h: fluorescence blue light). (a,b: Huadian; c,d: Maoming; e,f: Wang18; g,h: Ordos), polished thin section, immersion oil objective, ×500, scale bar = 50 μm.

Fig. 3. Examples of RE6 pyrolysis traces at 15 K/min. (a: excluding the S1 peak and the cool down signal for the Maoming sample; b: traces after the signal has been trimmed, thinned and the baseline corrected for the Maoming sample; c: excluding the S1 peak and the cool down signal for the Wang18 sample; d: traces after signal has been trimmed, thinned and the baseline corrected for the Wang18 sample).

Fig. 4. A comparison of replicate RE6 runs at 5 K/min and 25 K/min (a) with optimized A and (b) with fixed A. (Note that two superimposed sets of measured data and two models are shown for each sample and each heating rate. Traces normalized to the measured data instead of the model. a: Huadian; b: Maoming; c: Wang18; d: Ordos). Resulting optimized kinetics solutions calculated using one or the other of the replicate data sets similarly provided essentially identical results.

Fig. 5. Initial potential (Xi) histograms for fixed A (3×10^{13}/s) solutions for group W_1 heating rates (1, 15, 40 K/min. a: Huadian; b: Maoming; c: Wang18; d: Ordos).

Fig. 6. Initial potential (Xi) and activation energy distributions calculated for each sample with the frequency factor (A) optimized for heating rate group W_1 by (a) RE6 and (b) SRA. (a: Huadian; b: Maoming; c: Wang18; d: Ordos).

Fig. 7. Comparison of the measured data (symbols) and calculated or predicted hydrocarbon yield (curve) for heating rate group W_1 (1, 15 and 40 K/min) for (a) optimized A and (b) fixed A. (a: Huadian; b: Maoming; c: Wang18; d: Ordos).

Fig. 8. Comparison of the calculated cumulative HC generation at geological heating rates of 1,3 and 10 K/Ma for kinetics solutions derived for the low heating rate group (1, 2 and 5K/min) and A optimized for (a) Huadian, (b) Maoming, (c) Wang18 and (d) Ordos.

Fig. 9. A comparison of the predicted cumulative hydrocarbon generation at 3 K/Ma for each of the samples and for each of the heating rates groups from the two labs (L: 1, 2 and 5 K/min; H: 15, 25 and 40 K/min; W_1: 1, 15 and 40 K/min; W_2:2, 15 and 40K/min for Wuxi and 0.7, 2.0 and 5.0 K/min for GFZ. a: Huadian; b: Maoming; c: Wang18; d: Ordos).

Fig. 10. Temperatures predicted for 50% TR of samples heated at 3 K/Ma as a function of the heating rates used to optimize a kinetics solution.(a: Huadian; b: Maoming; c: Wang18; d: Ordos). Peters et al. (2015) have indicated that solutions Wide1 or Wide2 should provide the best models because these have heating rates that differ by 40× and 20×, respectively. The GFZ-low solution has the lowest heating rate range (0.7–5 K/min) but only a 7.1×ratio. The Low heating rates (Wuxi: 1, 2 and 5 K/min) have a slightly lower ratio of 5, but significantly lower predicted 50% TR temperature for three of the samples.

460

461 Tables

462 Table 1. Sample information.

463 Table 2. TOC, vitrinite reflectance and Rock-Eval pyrolysis results from Wuxi (a). TOC and
464 Rock-Eval results from GFZ (b). The different pyrolysis results between the two laboratories
465 reflect the fact that different subsamples of a heterogeneous hand specimen were analyzed in
466 the two labs. Despite the different pyrolysis results, the optimized kinetics were essentially
467 similar.

468 Table 3. Initial potential (Xi) and Ea with fixed A for heating group W1. Results for heating
469 groups L, H and W2 are shown in Appendix A tables.

470 Table 4. Initial potential (Xi) and Ea using optimized A for Wuxi and GFZ results along with Wuxi
471 pyrolysis results but using the GFZ optimized A in order to allow direct comparison of the Ea
472 distributions (a: Huadian; b: Maoming; c: Wang18; D: Ordos).

473 Table 5. Temperatures (°C) predicted for various transformation ratios at a geological heating
474 rate of 1, 3, 10 K/Ma using the kinetics solutions for the Low heating rate group and optimized
475 A.

476 Table 6. Temperatures (°C) predicted for various transformation ratios at a geological heating
477 rate of 3 K/Ma using the kinetics solutions at Low, High and Wide heating rate ranges and A
478 optimized from Wuxi and GFZ. For the 50%TR column the highest temperatures are in bold

numbers with shading and the lowest predicted temperatures are italicized to emphasize the lack of systematic impact of choosing different heating rate groups to optimize the kinetics solution.

EndNote References

1. Magoon, L. B. *Petroleum systems of the United States: US Geological Survey Bulletin*, 1988, **1870**, 2-15.
2. Magoon, L. B.; Dow, W. G. *The Petroleum System--From Source to Trap*, American Association of Petroleum Geologists, Tulsa, 1994.
3. Schenk, H. J.; Dieckmann, V. *Marine and Petroleum Geology*, 2004, **21**, 79-95.
4. Peters, K. E.; Burnham, A. K.; Walters, C. C. *American Association of Petroleum Geologists Bulletin*, 2015, **99**, 591-616.
5. Sun, P.; Liu, Z.; Gratzer, R.; Xu, Y.; Liu, R.; Li, B.; Meng, Q.; Xu, J. *Oil Shale*, 2013, **30**, 402-418.
6. Xie, X.; Volkman, J. K.; Qin, J.; Borjigin, T.; Bian, L.; Zhen, L. *International Journal of Coal Geology*, 2014, **124**, 36-47.
7. Sun, P.; Liu, Z.; Li, B.; Liu, R.; Meng, Q.; Zhou, R.; Yao, S.; Xu, Y. *Journal of Jilin University (Earth Science Edition)*, 2012, **42**, 948-960.
8. Feng, X.; Oskolski, A. A.; Jin, J. *Review of Palaeobotany and Palynology*, 2011, **174**, 101-105.
9. Liu, X.; Gao, Q.; Jin, J. *Journal of Systematics and Evolution*, 2015, **53**, 297-307.
10. Zhu, J. M. Sc. Dissertation, Jilin University, 2007.
11. Zhang, S.; Zhu, G.; Liang, Y.; Dai, J.; Liang, H.; Li, M. *Organic Geochemistry*, 2005, **36**, 1717-1730.
12. Li, S.; Pang, X.; Li, M.; Jin, Z. *Organic Geochemistry*, 2003, **34**, 389-412.
13. Pang, X.; Li, M.; Li, S.; Jin, Z. *Organic Geochemistry*, 2003, **34**, 931-950.
14. Zhang, W.-Z.; Yang, H.; Li, S.-p. *Petroleum Exploration and Development*, 2008, **35**, 557-562.
15. Yao, J.; Deng, X.; Zhao, Y.; Han, T.; Chu, M.; Pang, J. *Petroleum Exploration and Development*, 2013, **40**, 161-169.

16. Chen, L.; Lu, Y. presented in part at the 2014 GSA Annual Meeting, Vancouver, British Columbia, 19–22 October 2014, 2014.
17. Xie, X. M.; Tenger; Yang, Y. F.; Hu, M. X.; Bian, L. Z. *Petroleum Geology and Experiment*, 2013, **35**, 468-472.
18. Espitalié, J.; Deroo, G.; Marquis, F. *Oil & Gas Science and Technology – Rev. IFP Energies nouvelles*, 1985, **1**, 563-579.
19. Espitalié, J.; Deroo, G.; Marquis, F. *Oil & Gas Science and Technology – Rev. IFP Energies nouvelles*, 1985, **40**.
20. Espitalié, J.; Deroo, G.; Marquis, F. *Oil & Gas Science and Technology – Rev. IFP Energies nouvelles*, 1985, **41**, 73-89.
21. Lafargue, E.; Espitalié, J.; Marquis, F.; Pillot, D. *Revue de l'Institut Francais du Petrole*, 1998, **53**, 421-437.
22. Petersen, H. I. *International Journal of Coal Geology*, 2006, **67**, 221-248.
23. Fuhrmann, A.; Horsfield, B.; Lòpez, J. F.; Hu, L.; Zhang, Z. *Journal of Petroleum Geology*, 2004, **27**, 27-46.

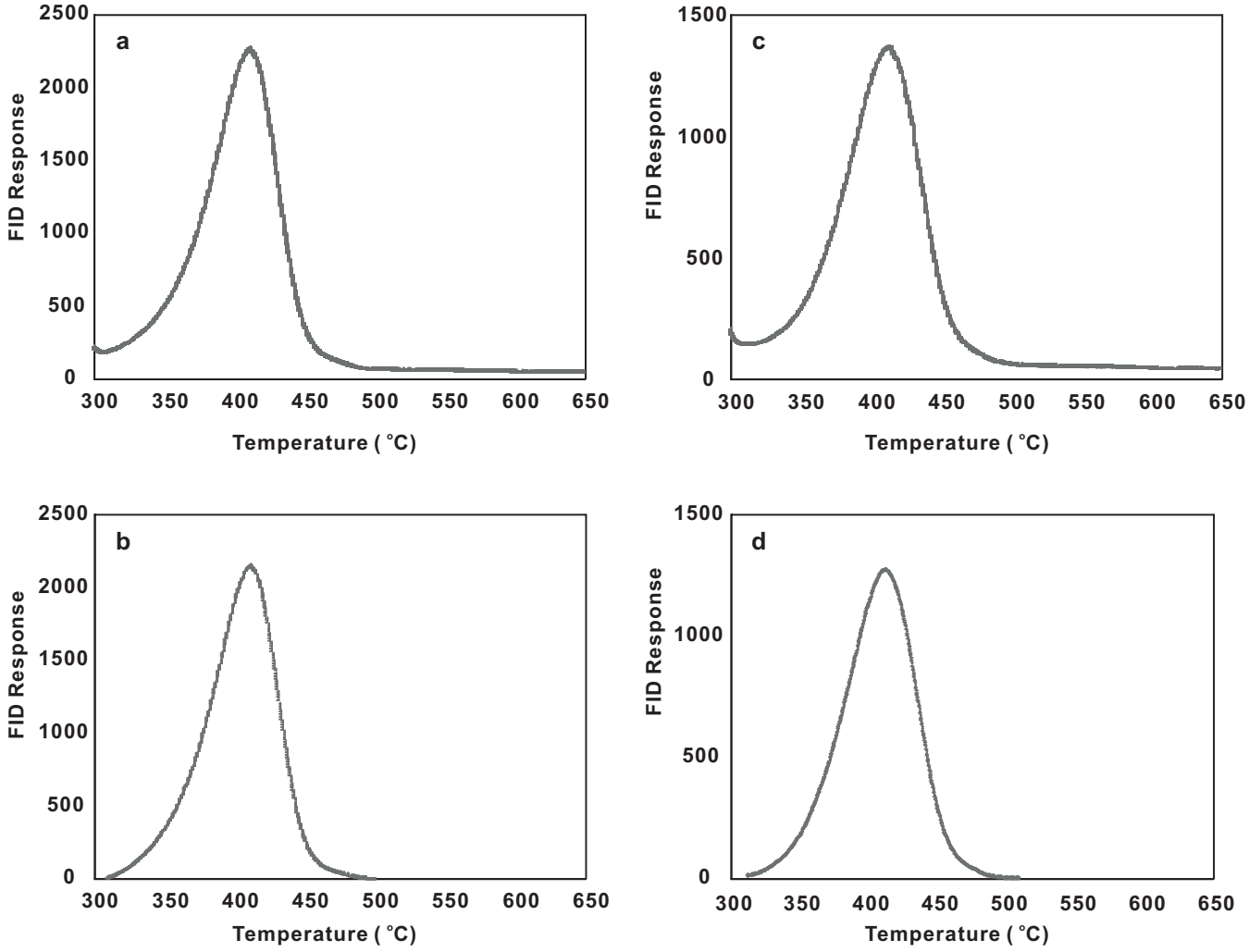

Fig. A1a. Examples of RE6 pyrolysis traces at 1 K/min.(a: excluding the S1 peak and the cool down signal for the Maoming sample; b: traces after signal has been trimmed, thinned and the baseline corrected for the Maoming sample; c: excluding the S1 peak and the cool down signal for the Wang18 sample; d: traces after signal has been trimmed, thinned and the baseline corrected for the Wang18 sample).

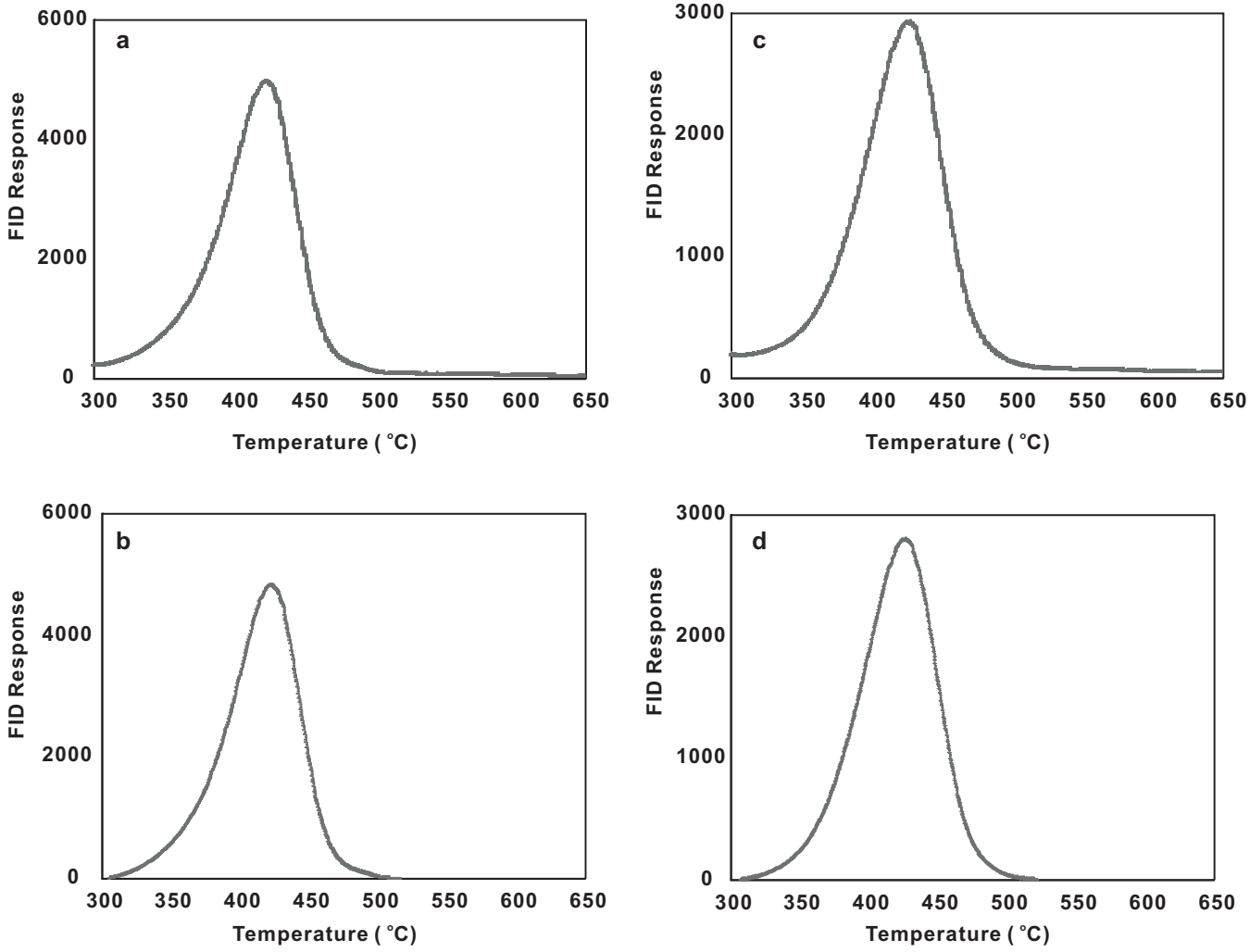

Fig. A1b. Examples of RE6 pyrolysis traces at 2 K/min.(a: excluding the S1 peak and the cool down signal for the Maoming sample; b: traces after signal has been trimmed, thinned and the baseline corrected for the Maoming sample; c: excluding the S1 peak and the cool down signal for the Wang18 sample; d: traces after signal has been trimmed, thinned and the baseline corrected for the Wang18 sample).

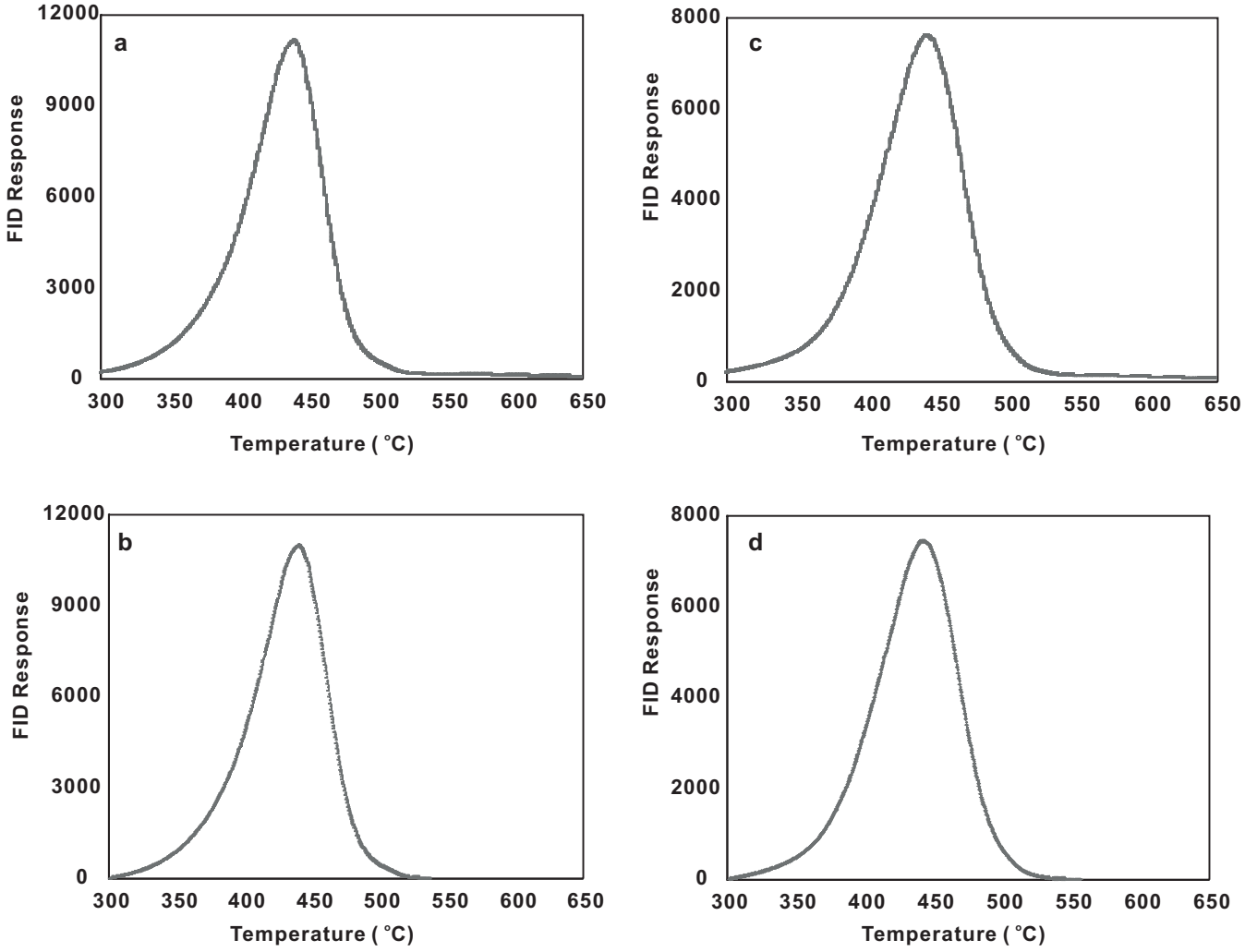

Fig. A1c. Examples of RE6 pyrolysis traces at 5 K/min.(a: excluding the S1 peak and the cool down signal for the Maoming sample; b: traces after signal has been trimmed, thinned and the baseline corrected for the Maoming sample; c: excluding the S1 peak and the cool down signal for the Wang18 sample; d: traces after signal has been trimmed, thinned and the baseline corrected for the Wang18 sample).

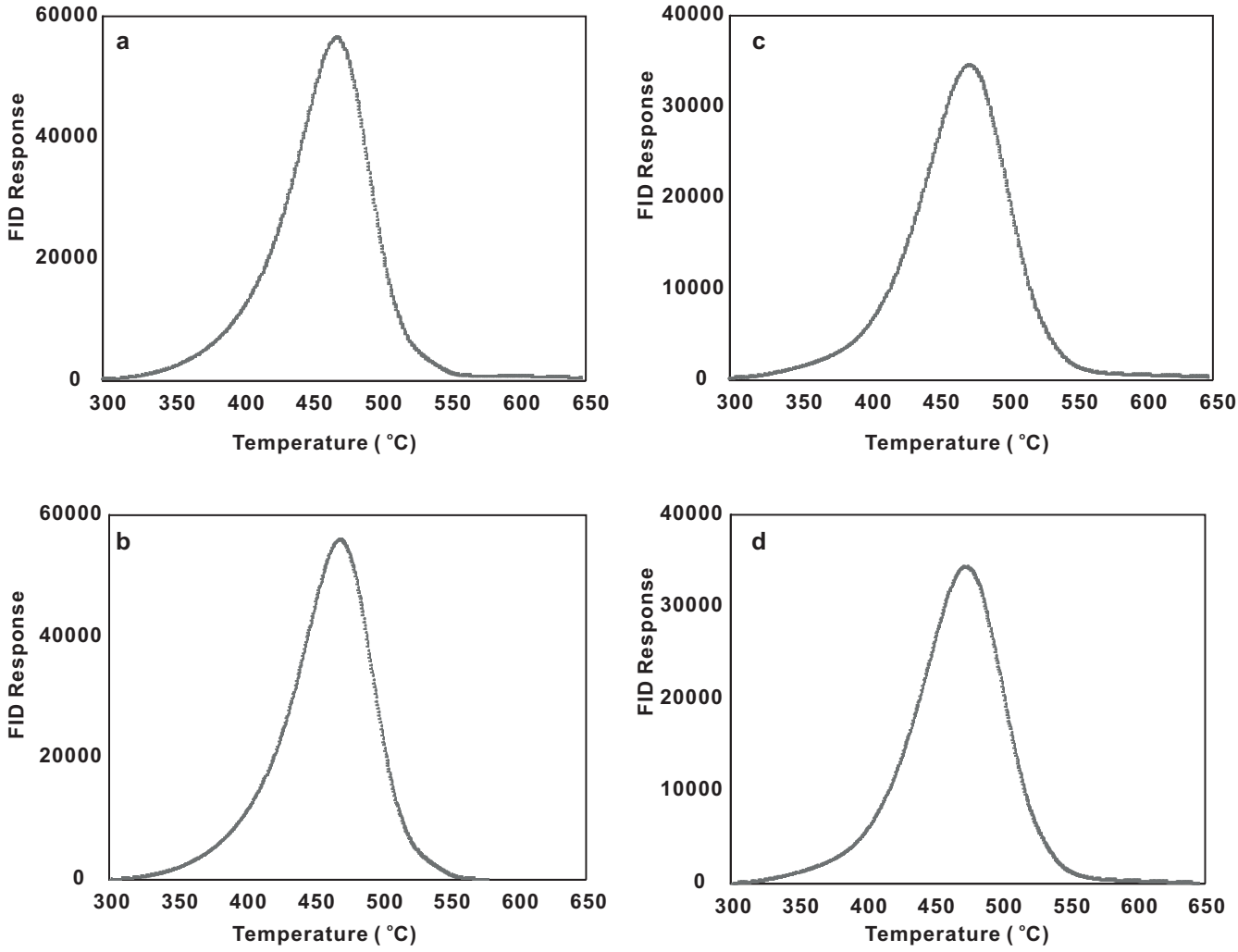

Fig. A1d. Examples of RE6 pyrolysis traces at 25 K/min.(a: excluding the S1 peak and the cool down signal for the Maoming sample; b: traces after signal has been trimmed, thinned and the baseline corrected for the Maoming sample; c: excluding the S1 peak and the cool down signal for the Wang18 sample; d: traces after signal has been trimmed, thinned and the baseline corrected for the Wang18 sample).

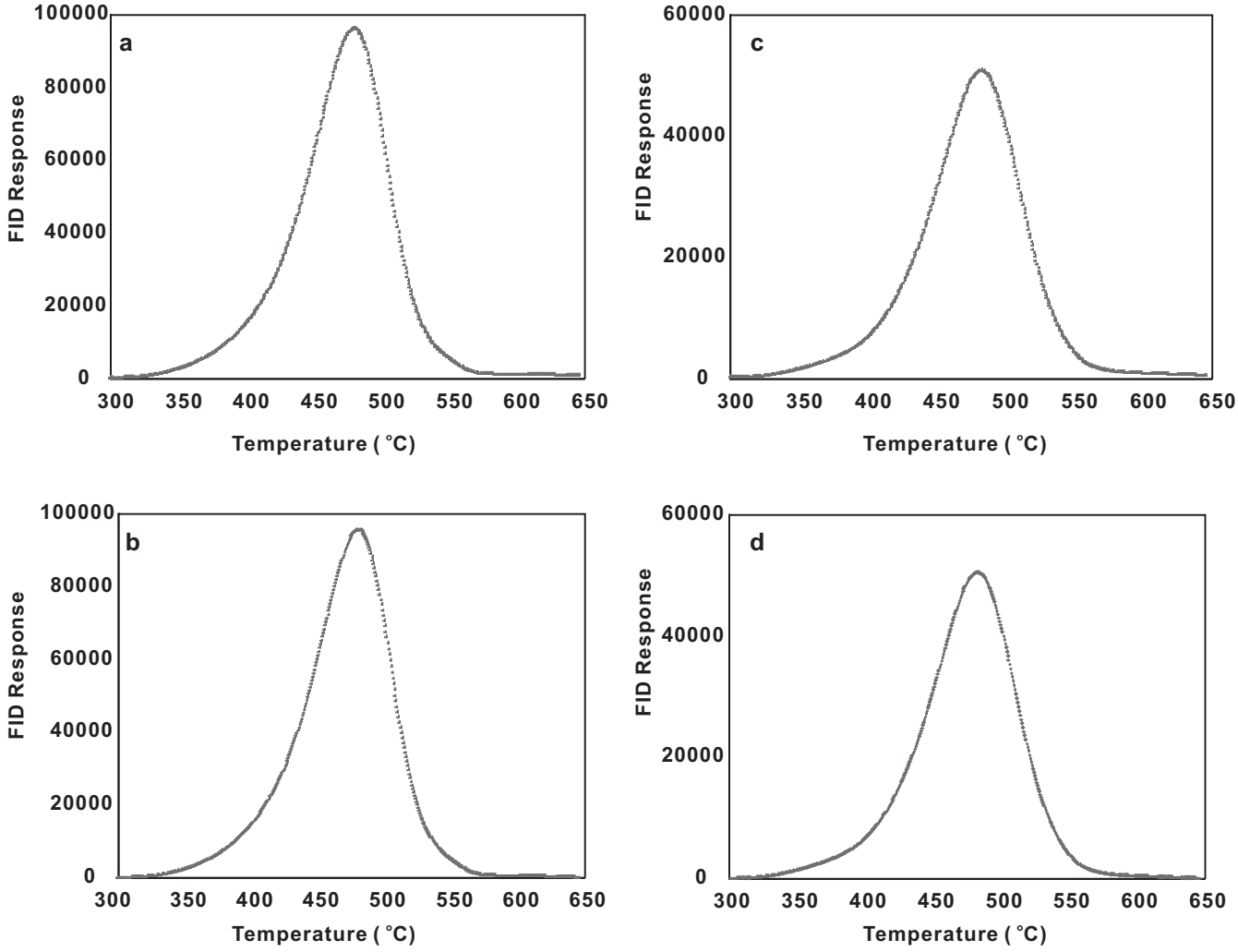

Fig. A1e. Examples of RE6 pyrolysis traces at 40 K/min.(a: excluding the S1 peak and the cool down signal for the Maoming sample; b: traces after signal has been trimmed, thinned and the baseline corrected for the Maoming sample; c: excluding the S1 peak and the cool down signal for the Wang18 sample; d: traces after signal has been trimmed, thinned and the baseline corrected for the Wang18 sample).

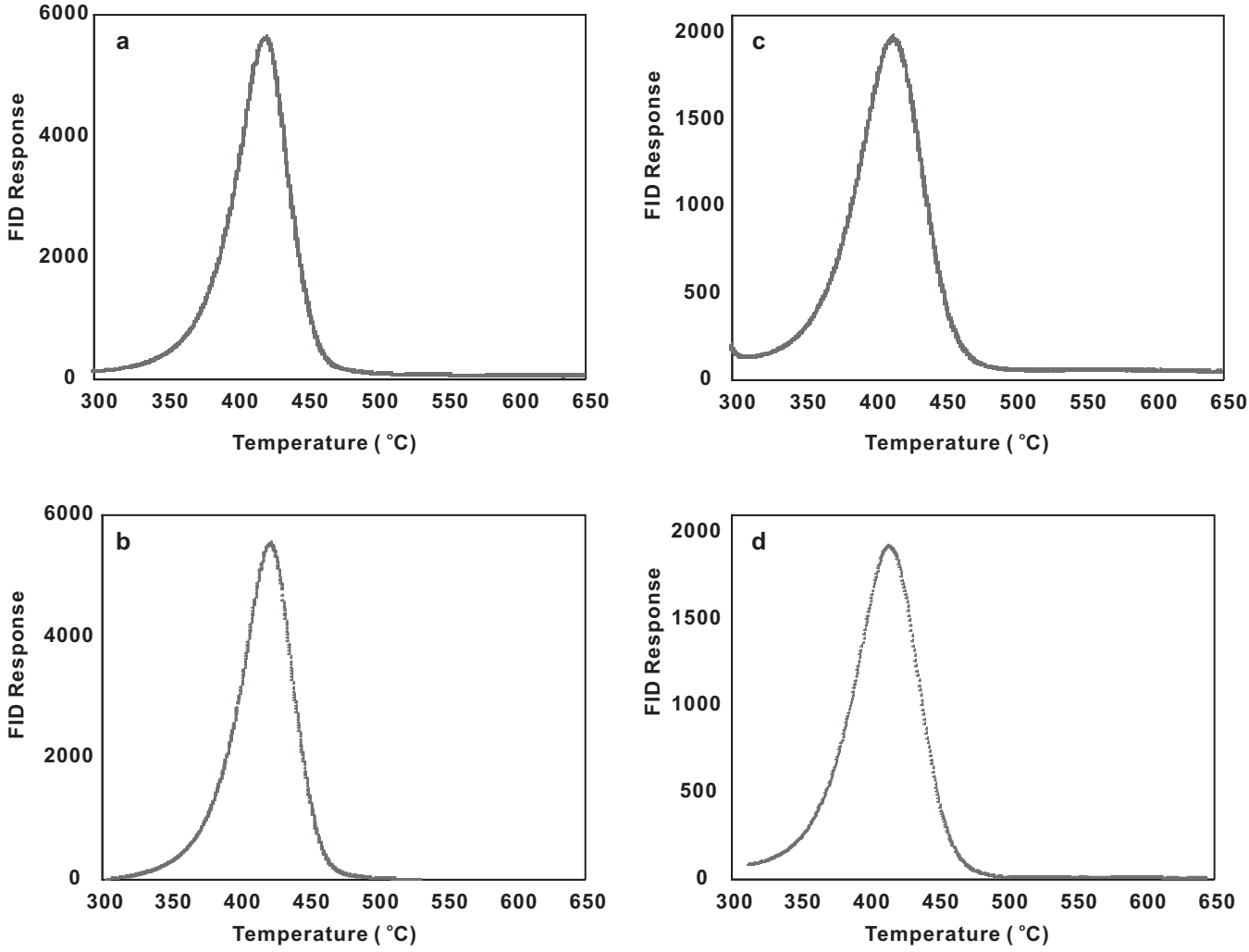

Fig. A1f. Examples of RE6 pyrolysis traces at 1 K/min.(a: excluding the S1 peak and the cool down signal for the Huadian sample; b: traces after signal has been trimmed, thinned and the baseline corrected for the Huadian sample; c: excluding the S1 peak and the cool down signal for the Ordos sample; d: traces after signal has been trimmed, thinned and the baseline corrected for the Ordos sample).

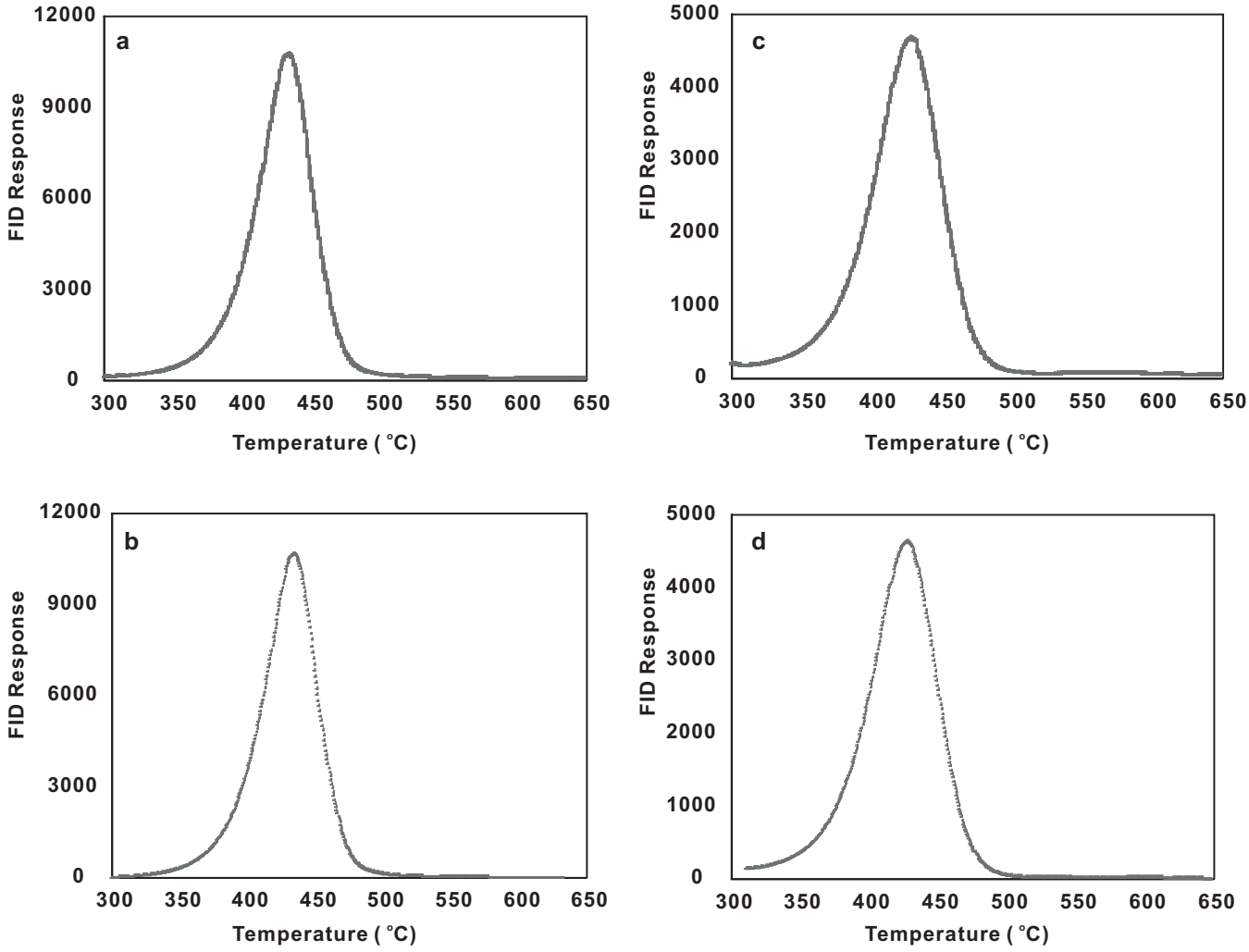

Fig. A1g. Examples of RE6 pyrolysis traces at 2 K/min.(a: excluding the S1 peak and the cool down signal for the Huadian sample; b: traces after signal has been trimmed, thinned and the baseline corrected for the Huadian sample; c: excluding the S1 peak and the cool down signal for the Ordos sample; d: traces after signal has been trimmed, thinned and the baseline corrected for the Ordos sample).

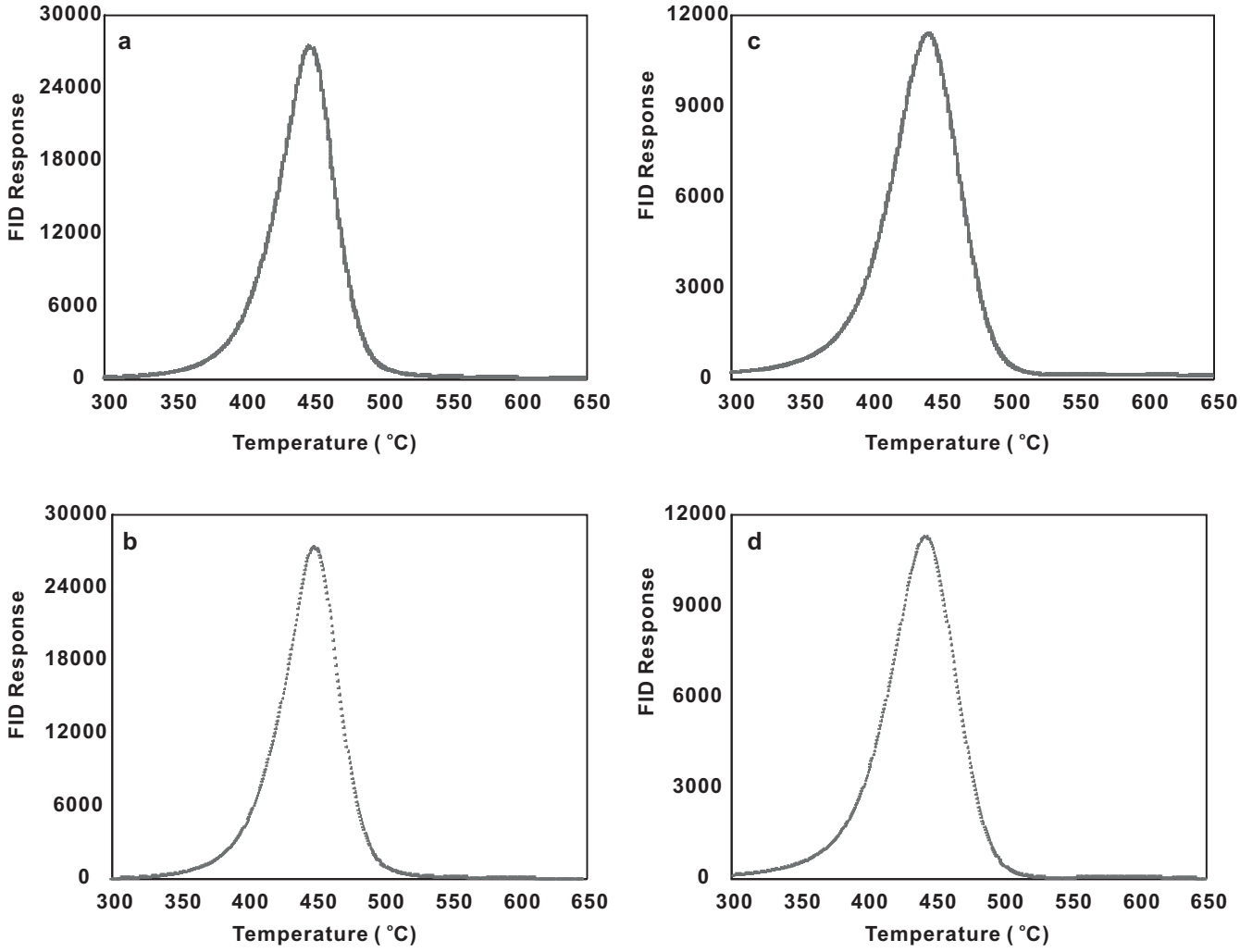

Fig. A1h. Examples of RE6 pyrolysis traces at 5 K/min.(a: excluding the S1 peak and the cool down signal for the Huadian sample; b: traces after signal has been trimmed, thinned and the baseline corrected for the Huadian sample; c: excluding the S1 peak and the cool down signal for the Ordos sample; d: traces after signal has been trimmed, thinned and the baseline corrected for the Ordos sample).

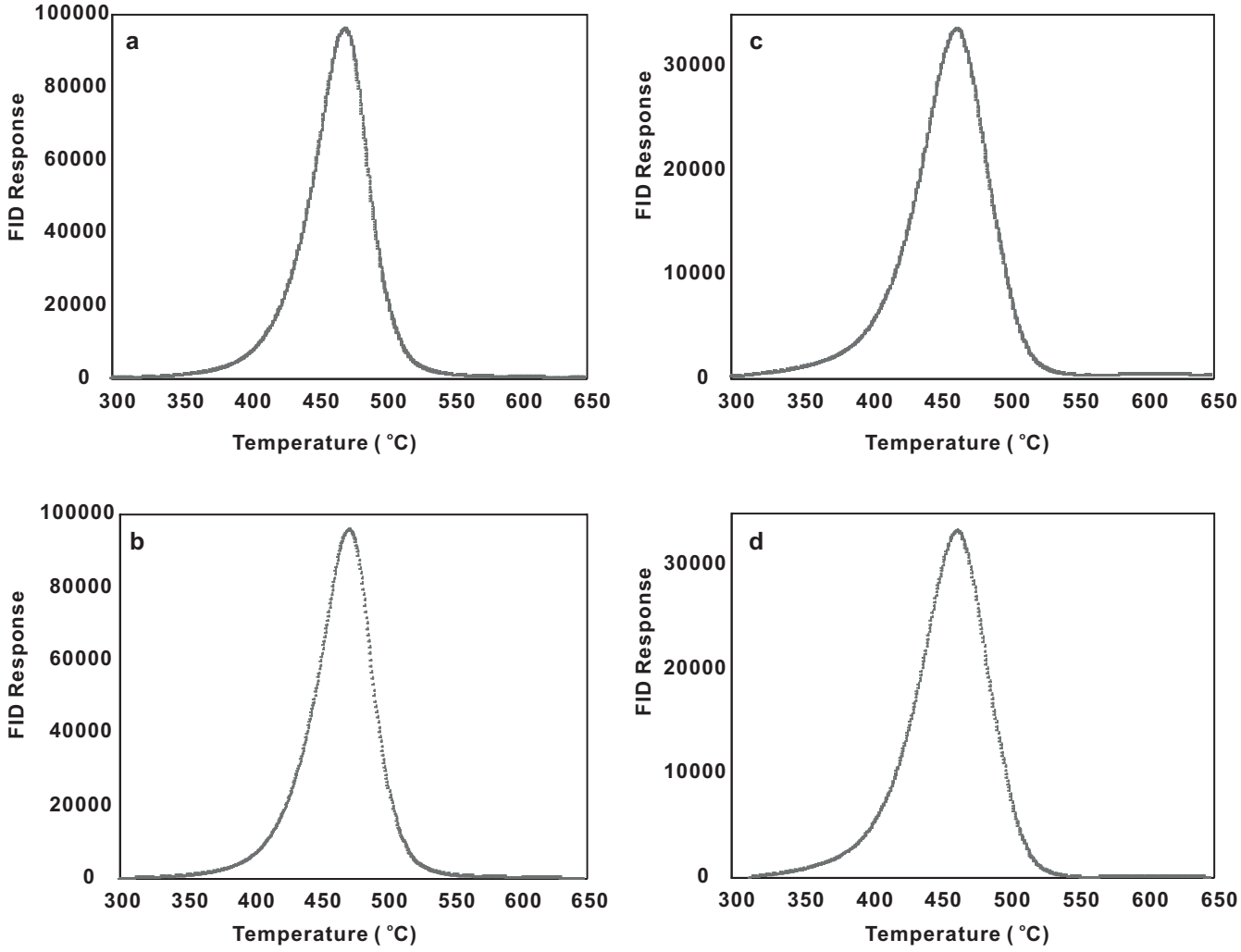

Fig. A1i. Examples of RE6 pyrolysis traces at 15 K/min.(a: excluding the S1 peak and the cool down signal for the Huadian sample; b: traces after signal has been trimmed, thinned and the baseline corrected for the Huadian sample; c: excluding the S1 peak and the cool down signal for the Ordos sample; d: traces after signal has been trimmed, thinned and the baseline corrected for the Ordos sample).

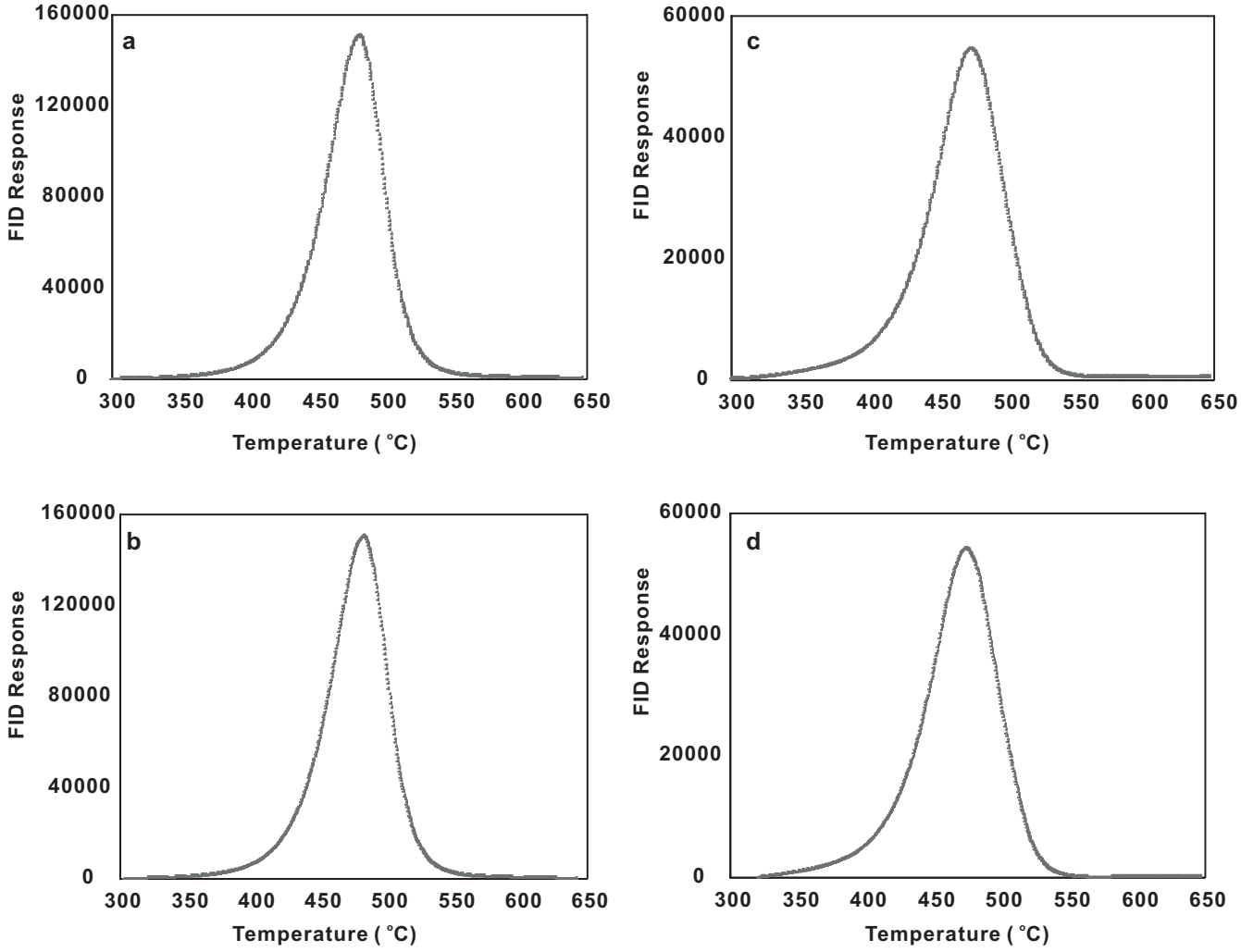

Fig. A1g. Examples of RE6 pyrolysis traces at 25 K/min.(a: excluding the S1 peak and the cool down signal for the Huadian sample; b: traces after signal has been trimmed, thinned and the baseline corrected for the Huadian sample; c: excluding the S1 peak and the cool down signal for the Ordos sample; d: traces after signal has been trimmed, thinned and the baseline corrected for the Ordos sample).

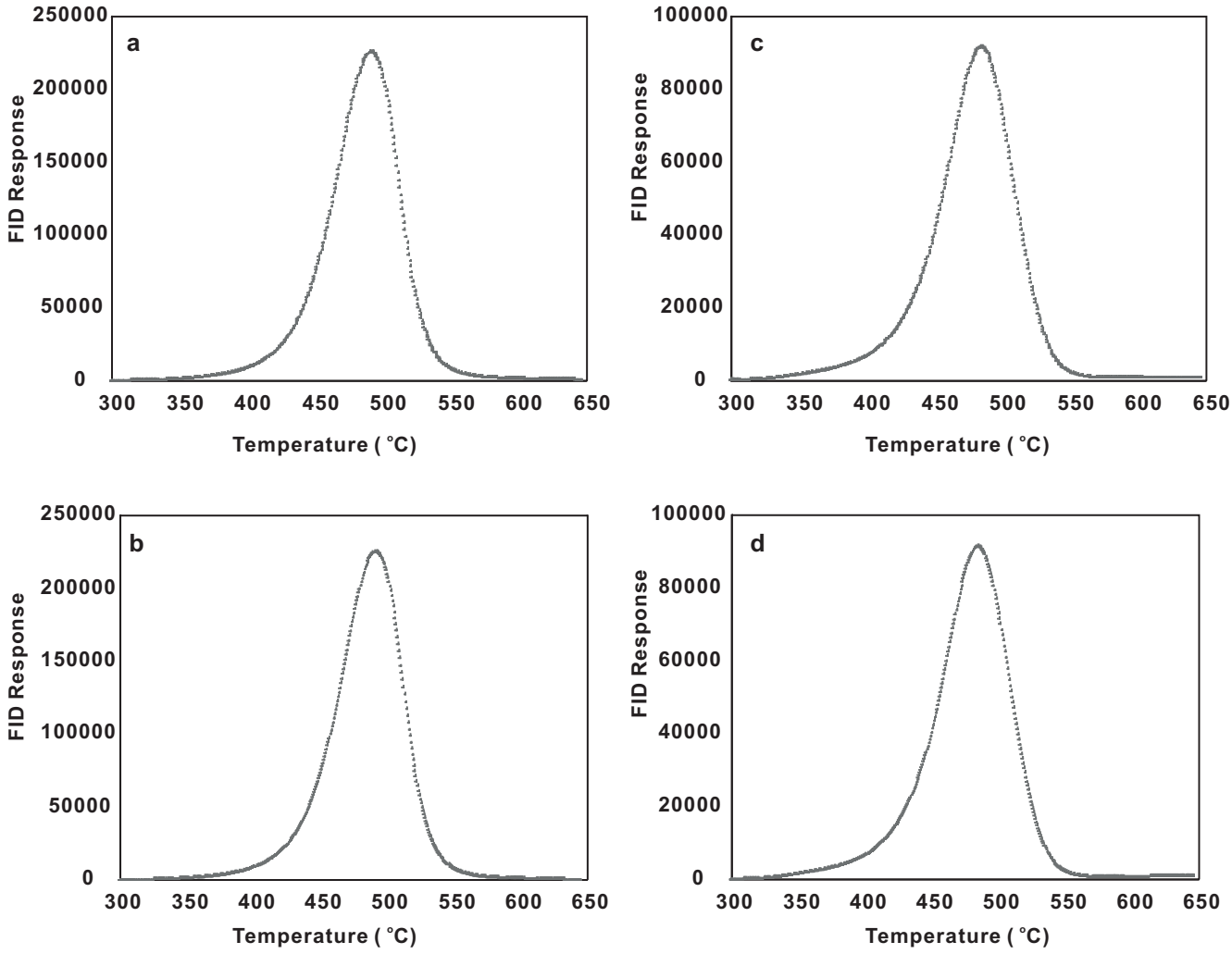

Fig. A1k. Examples of RE6 pyrolysis traces at 40 K/min.(a: excluding the S1 peak and the cool down signal for the Huadian sample; b: traces after signal has been trimmed, thinned and the baseline corrected for the Huadian sample; c: excluding the S1 peak and the cool down signal for the Ordos sample; d: traces after signal has been trimmed, thinned and the baseline corrected for the Ordos sample).

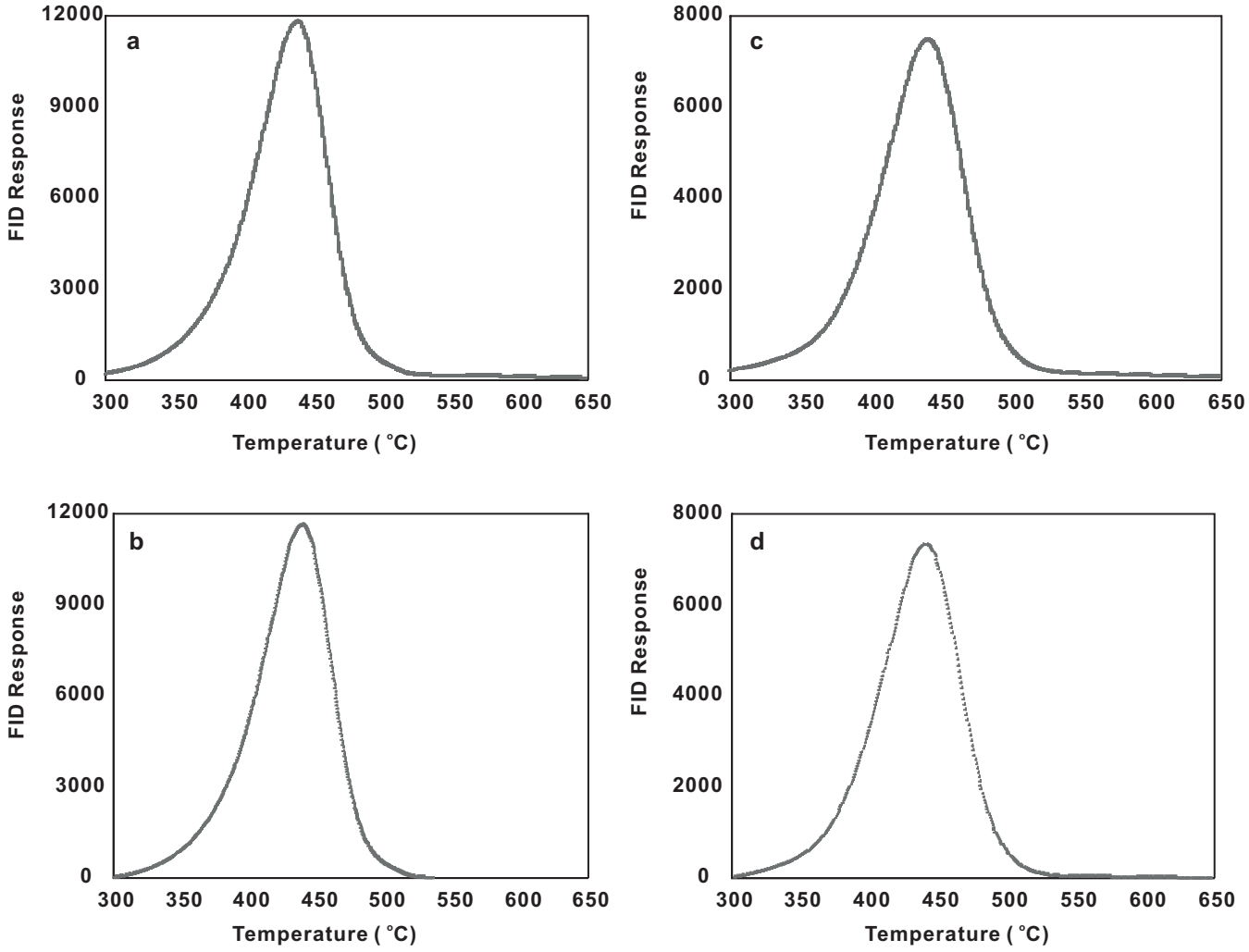

Fig. A1l. Examples of replicate RE6 pyrolysis traces at 5 K/min .(a: excluding the S1 peak and the cool down signal for the Maoming sample; b: traces after signal has been trimmed, thinned and the baseline corrected for the Maoming sample; c: excluding the S1 peak and the cool down signal for the Wang18 sample; d: traces after signal has been trimmed, thinned and the baseline corrected for the Wang18 sample).

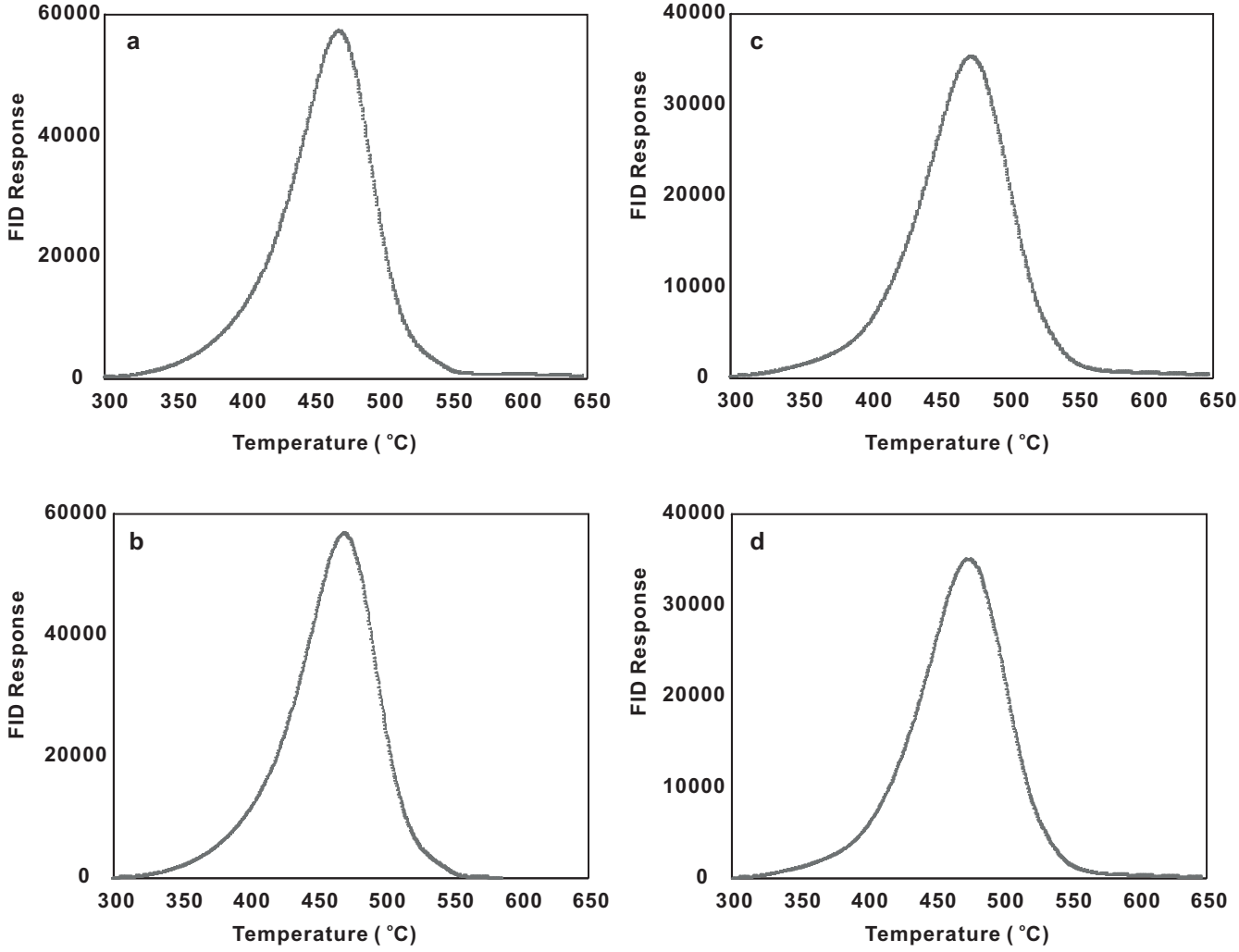

Fig. A1m. Examples of replicate RE6 pyrolysis traces at 25 K/min .(a: excluding the S1 peak and the cool down signal for the Maoming sample; b: traces after signal has been trimmed, thinned and the baseline corrected for the Maoming sample; c: excluding the S1 peak and the cool down signal for the Wang18 sample; d: traces after signal has been trimmed, thinned and the baseline corrected for the Wang18 sample).

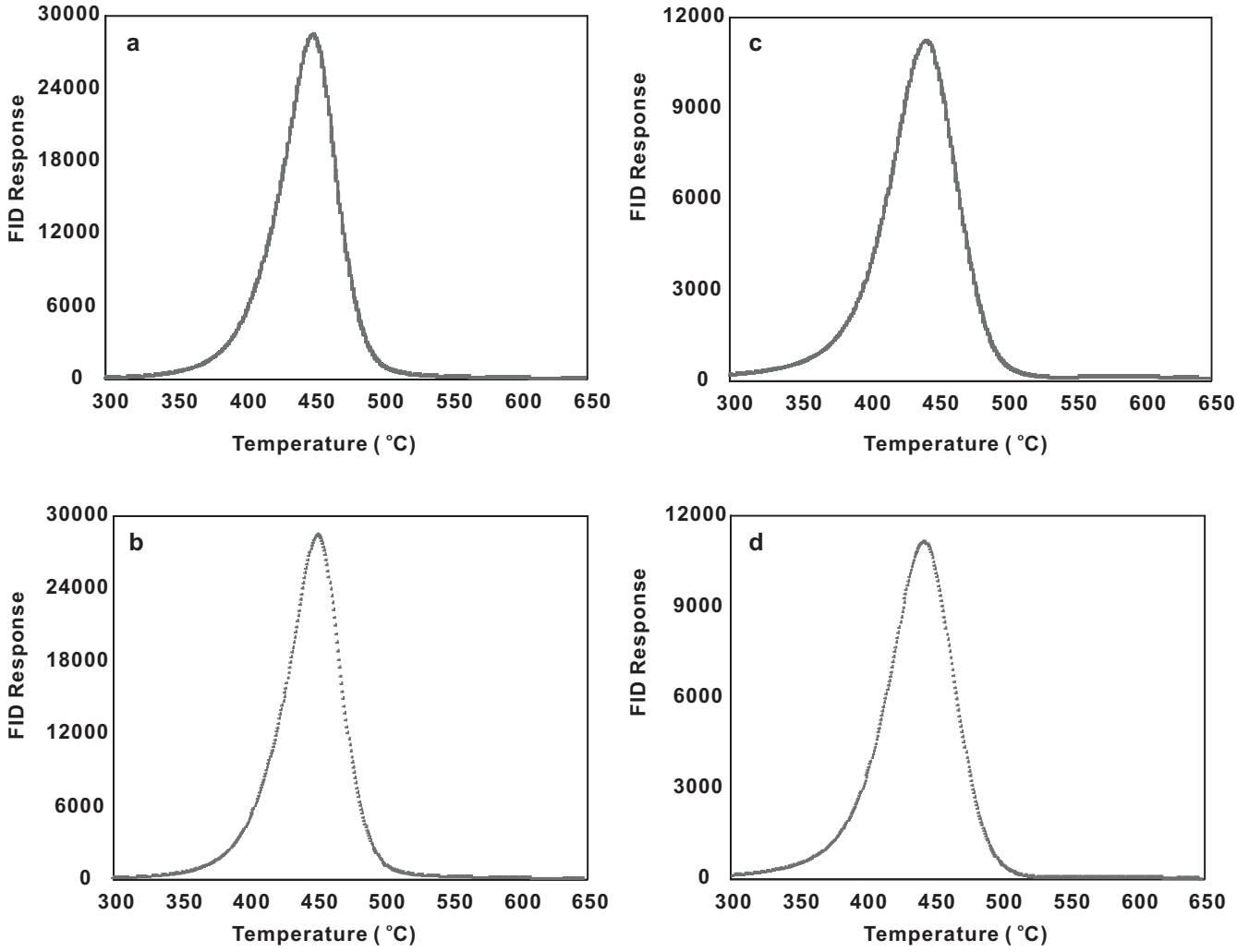

Fig. A1n. Examples of replicate RE6 pyrolysis traces at 5 K/min .(a: excluding the S1 peak and the cool down signal for the Huadian sample; b: traces after signal has been trimmed, thinned and the baseline corrected for the Huadian sample; c: excluding the S1 peak and the cool down signal for the Ordos sample; d: traces after signal has been trimmed, thinned and the baseline corrected for the Ordos sample).

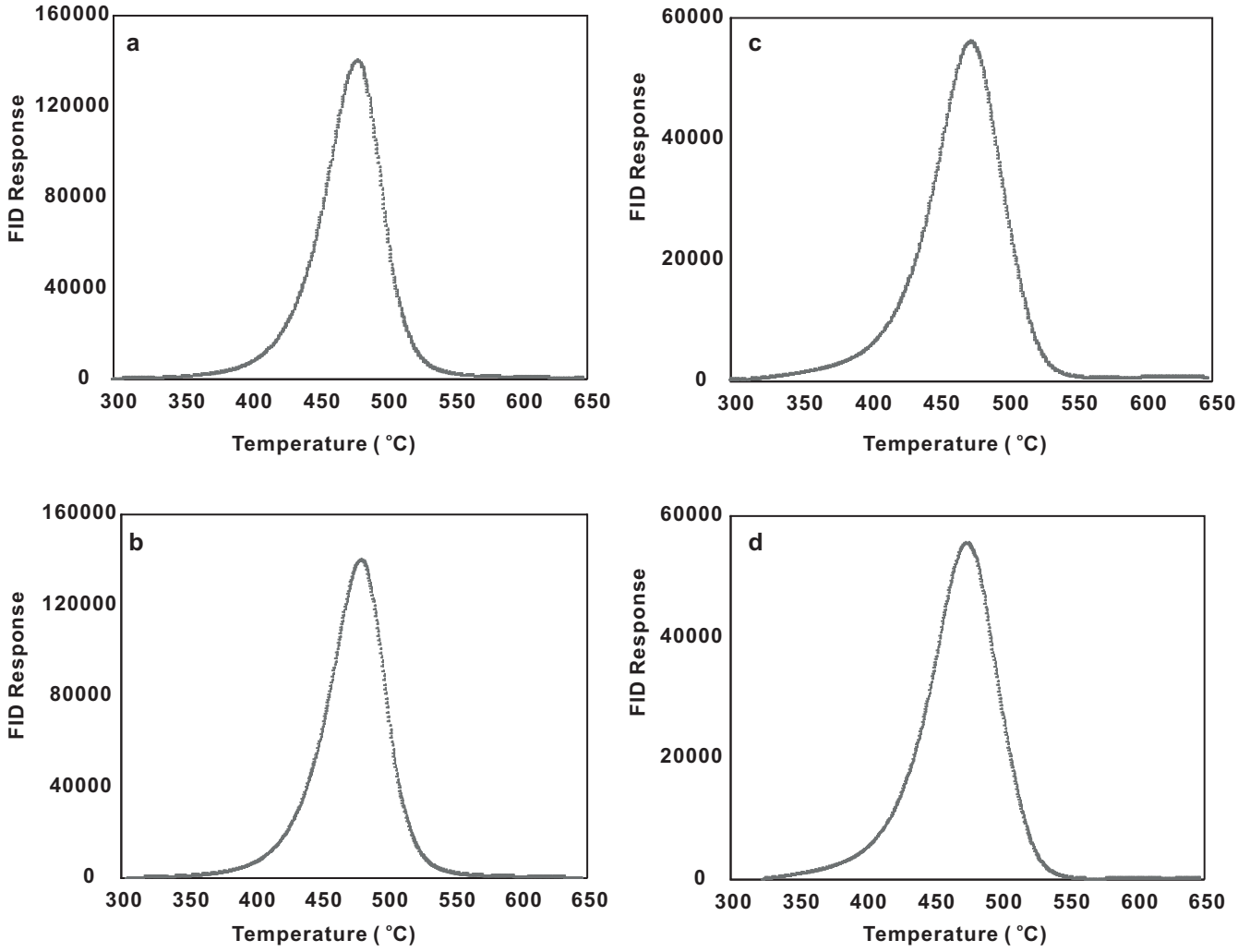

Fig. A1o. Examples of replicate RE6 pyrolysis traces at 25 K/min .(a: excluding the S1 peak and the cool down signal for the Huadian sample; b: traces after signal has been trimmed, thinned and the baseline corrected for the Huadian sample; c: excluding the S1 peak and the cool down signal for the Ordos sample; d: traces after signal has been trimmed, thinned and the baseline corrected for the Ordos sample).

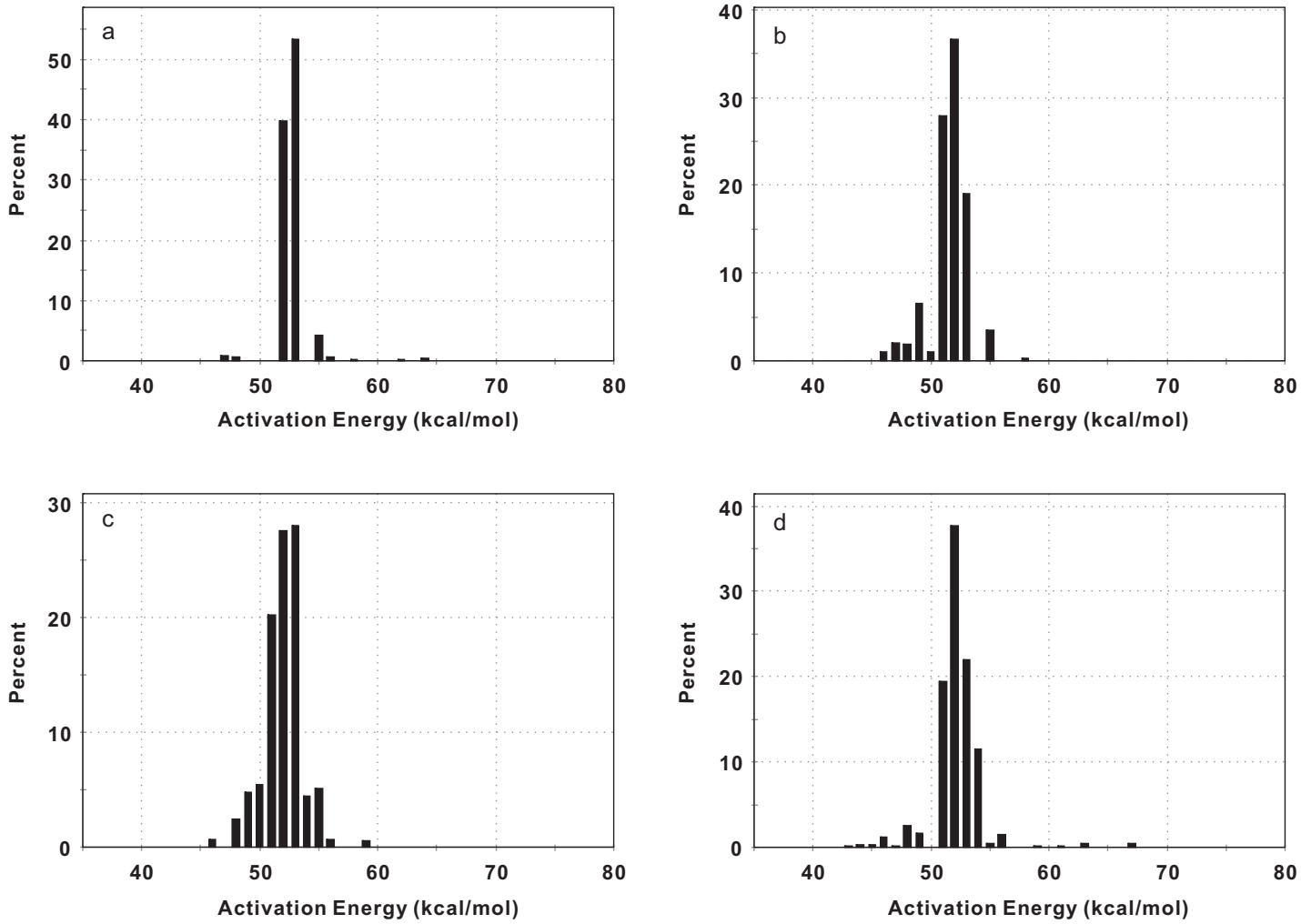

Fig. B1a Initial potential (Xi) histograms for fixed A (3×10^{13}/s) solutions for group L heating rates (1, 2 and 5 K/min. a: Huadian; b: Maoming; c: Wang18; d: Ordos).

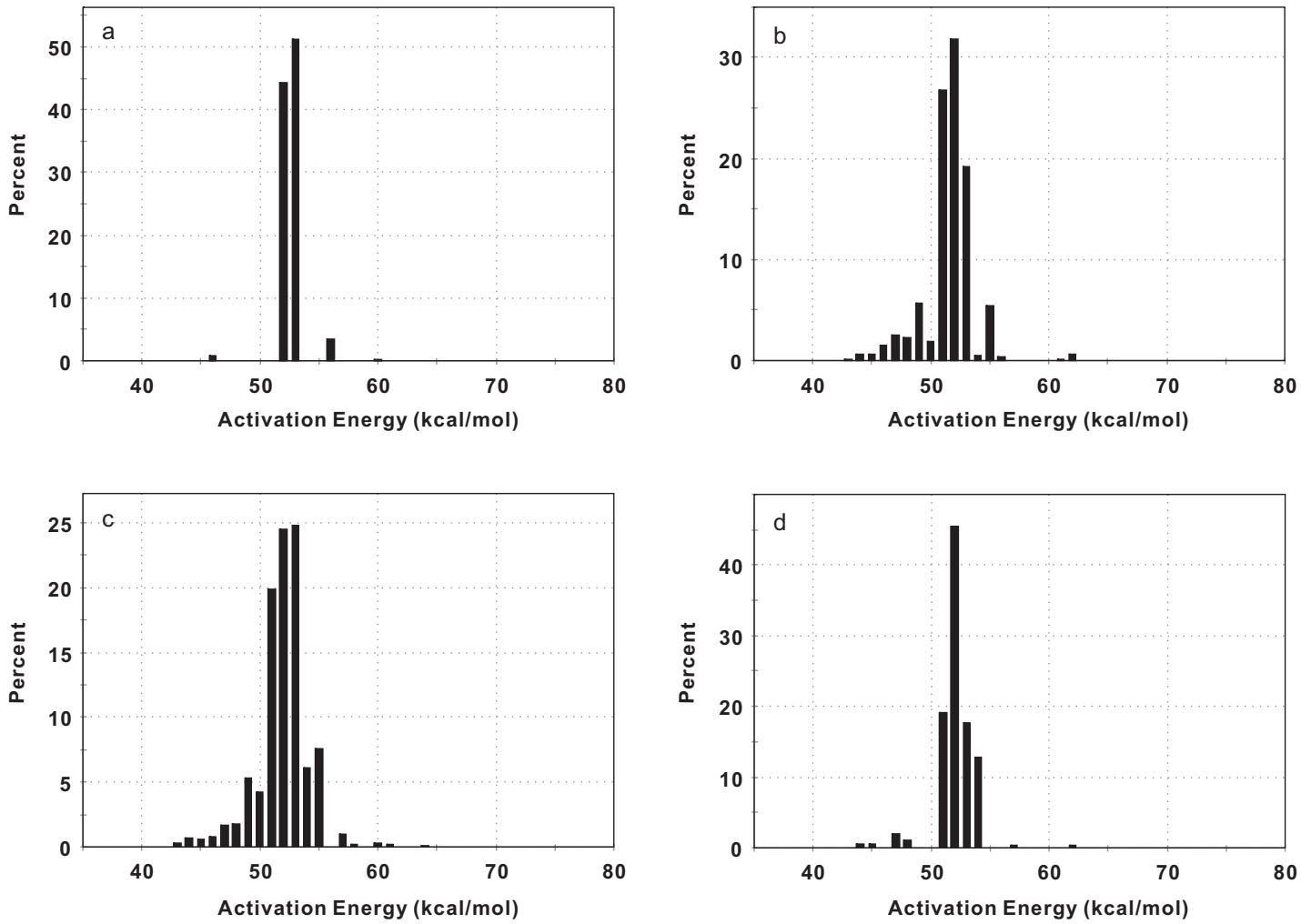

Fig. B1b Initial potential (X_i) histograms for fixed A (3×10^{13}/s) solutions for group H heating rates (15, 25 and 40 K/min. a: Huadian; b: Maoming; c: Wang18; d: Ordos).

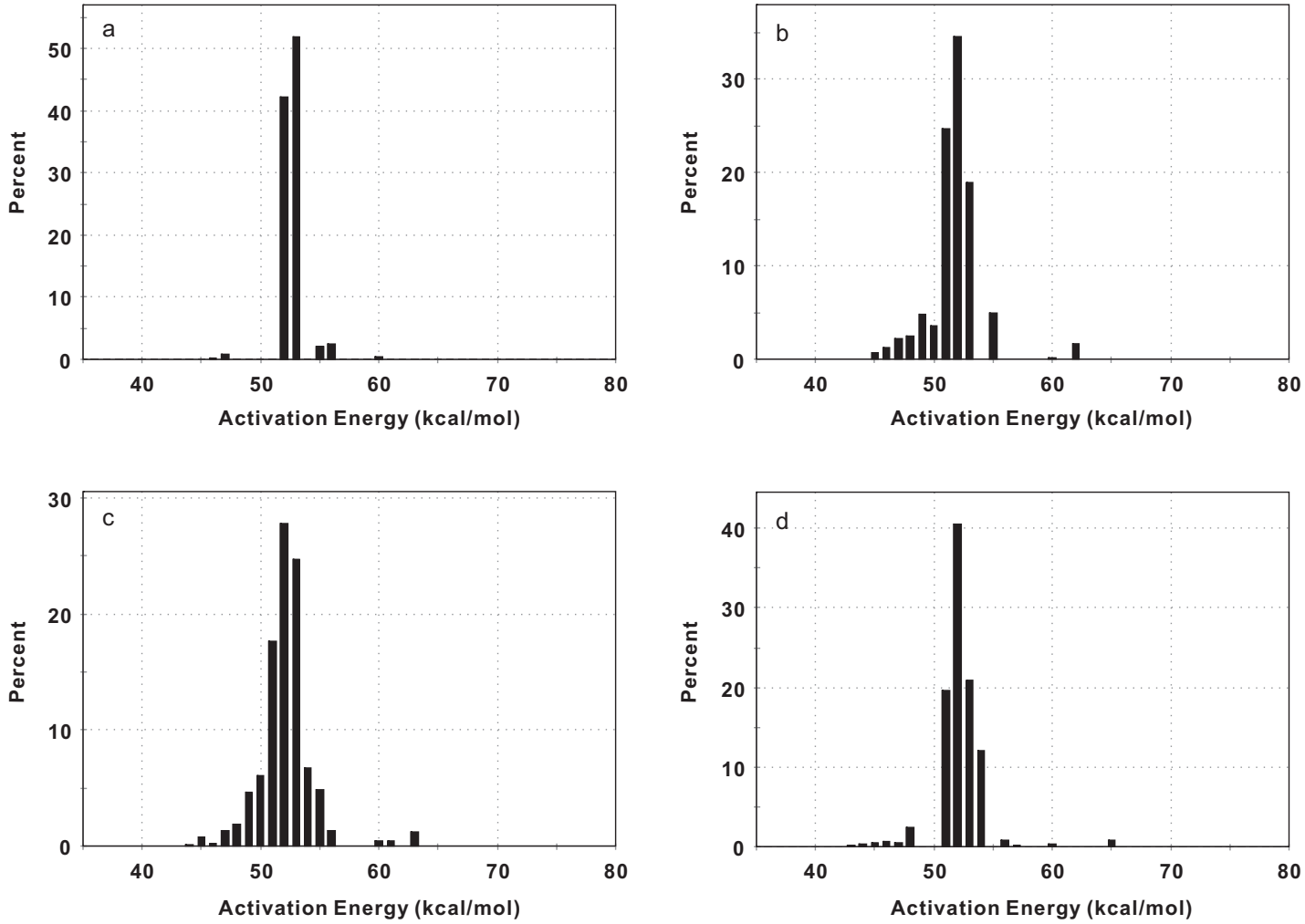

Fig. B1c Initial potential (X_i) histograms for fixed A (3×10^{13}/s) solutions for group W_2 heating rates (2, 15 and 40 K/min, a: Huadian; b: Maoming; c: Wang18; d: Ordos).

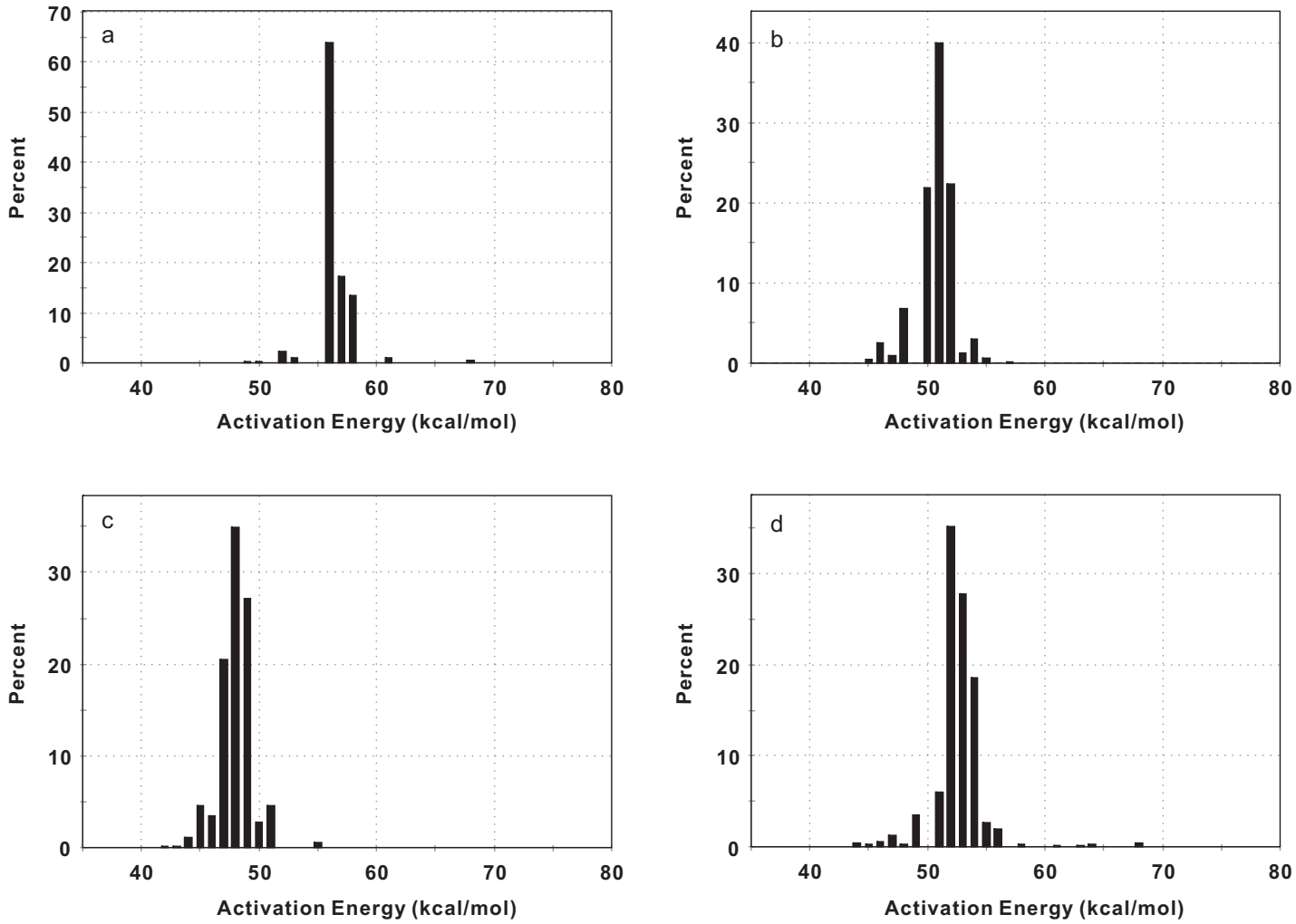

Fig.C1a Initial potential (X_i) and activation energy distributions calculated for each sample with the frequency factor (A) optimized at group L by Re6. (a: Huadian, A=4.59E+14; b: Maoming, A=1.63E+13; c: Wang18, A=1.57E+12; d: Ordos, A=4.24E+13).

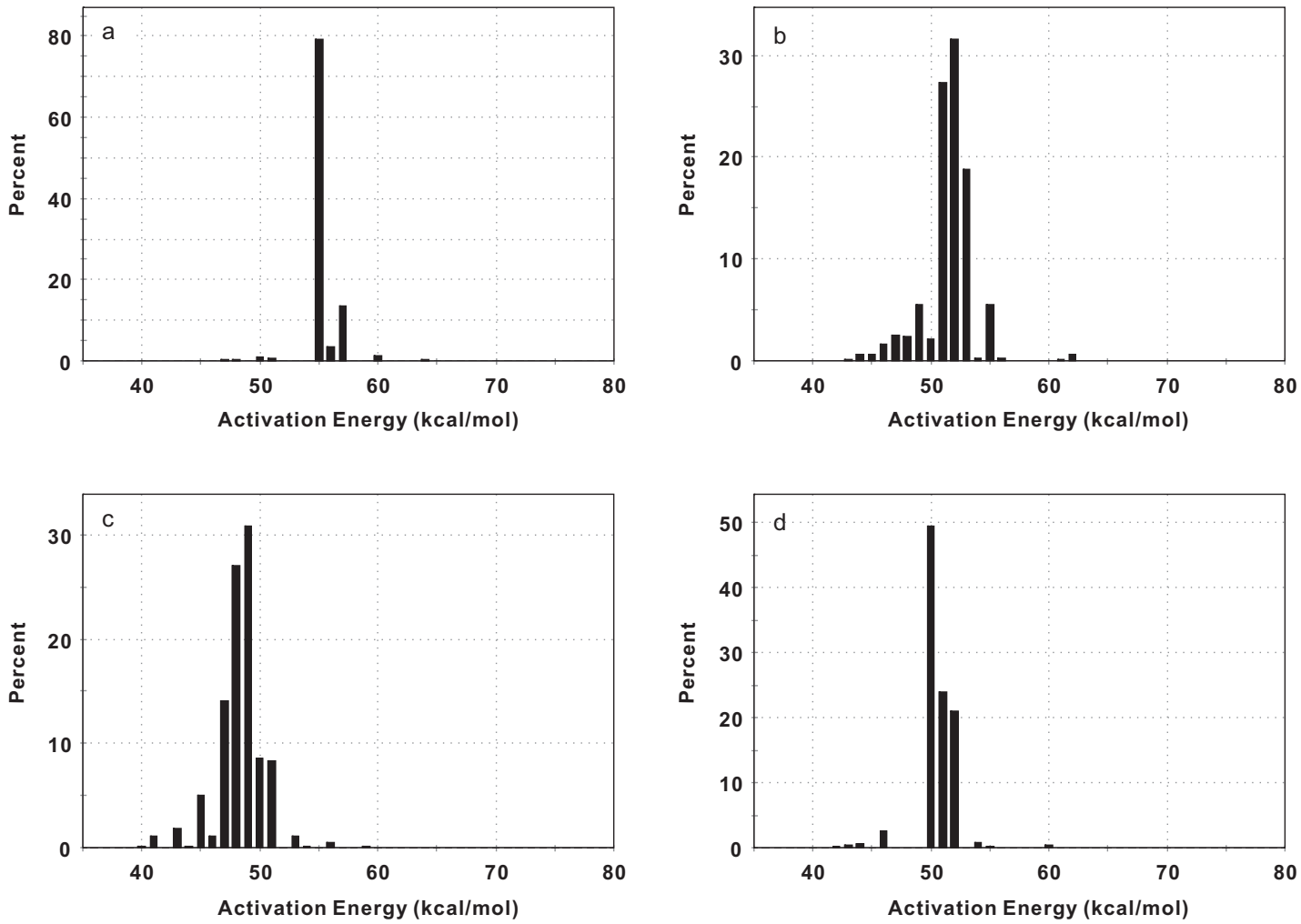

Fig.C1b Initial potential (X_i) and activation energy distributions calculated for each sample with the frequency factor (A) optimized at group H by RE6.

(a: Huadian, A=1.84E+14; b: Maoming, A=2.95E+13; c: Wang18, A=2.42E+12; d: Ordos, A=1.04E+13).

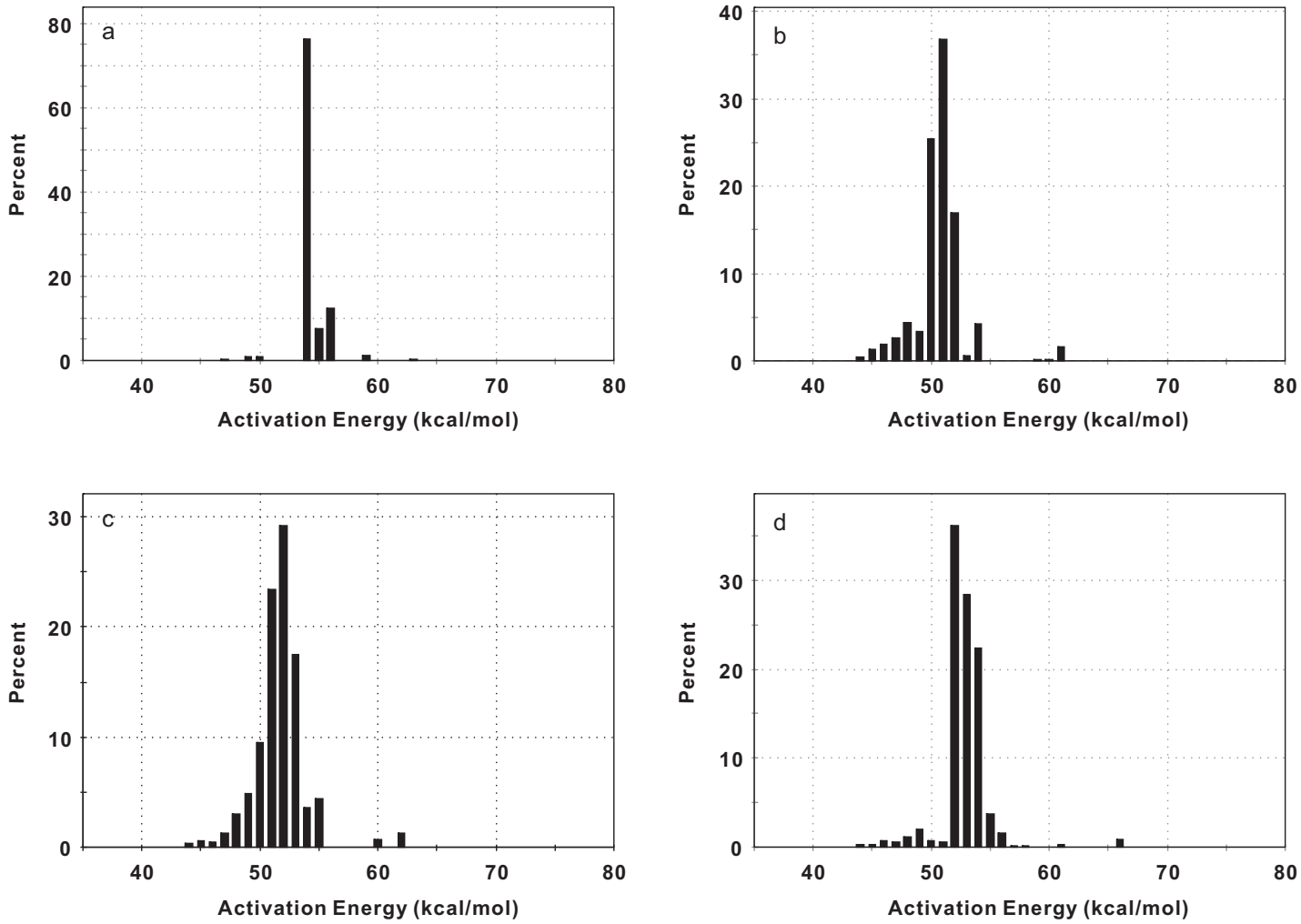

Fig.C1c Initial potential (X_i) and activation energy distributions calculated for each sample with the frequency factor (A) optimized at group W_2 by Re6. (a: Huadian, A=9.48E+13; b: Maoming, A=1.44E+13; c: Wang18, A=2.23E+13; d: Ordos, A=4.72E+13).

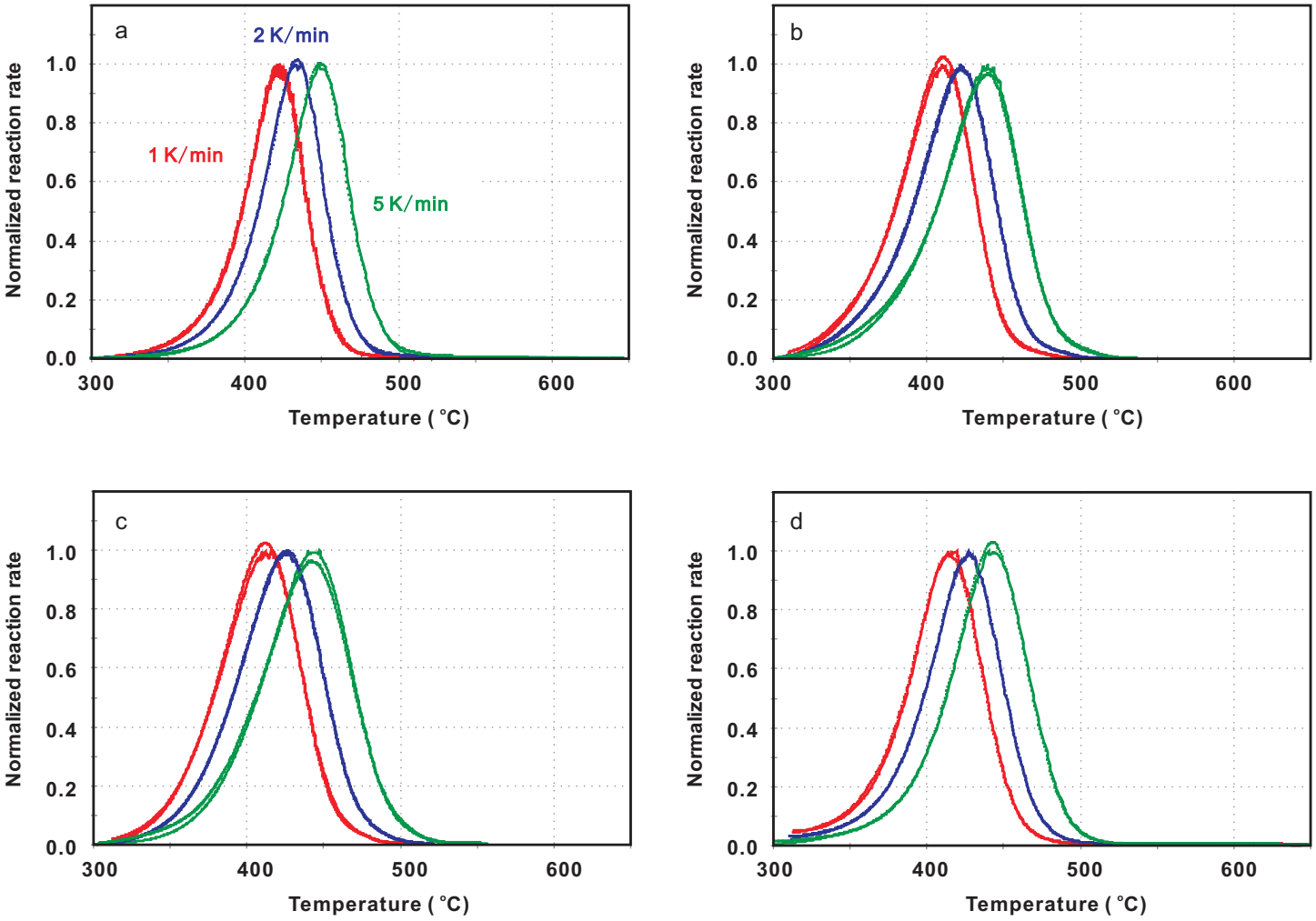

Fig. D1a Comparison of the measured data (symbols) and calculated or predicted hydrocarbon yield (curve) for heating rate group L. (with optimized A).
(a: Huadian; b: Maoming; c: Wang18; d: Ordos).

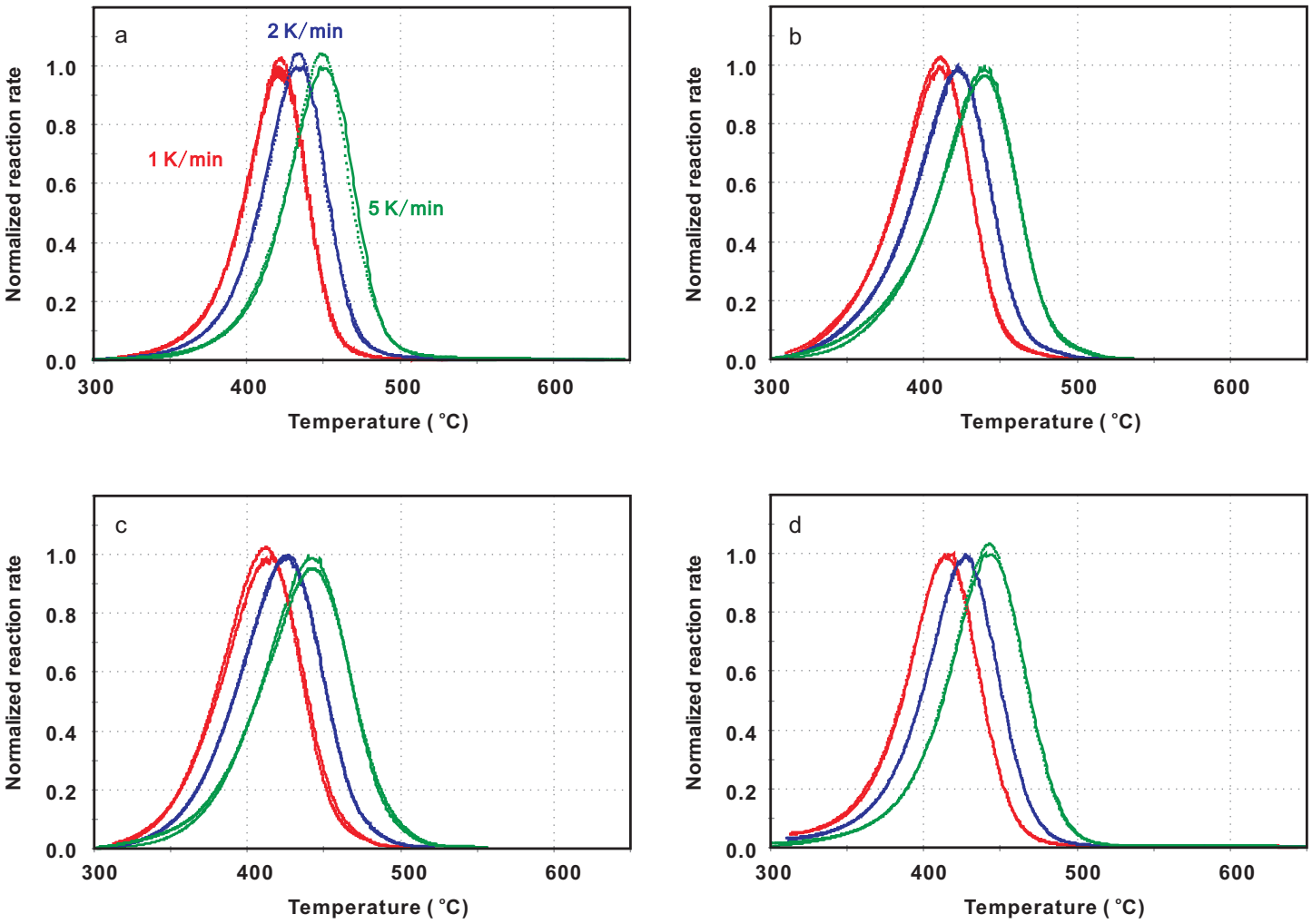

Fig. D1b Comparison of the measured data (symbols) and calculated or predicted hydrocarbon yield (curve) for heating rate group L. (with fixed A).
(a: Huadian; b: Maoming; c: Wang18; d: Ordos).

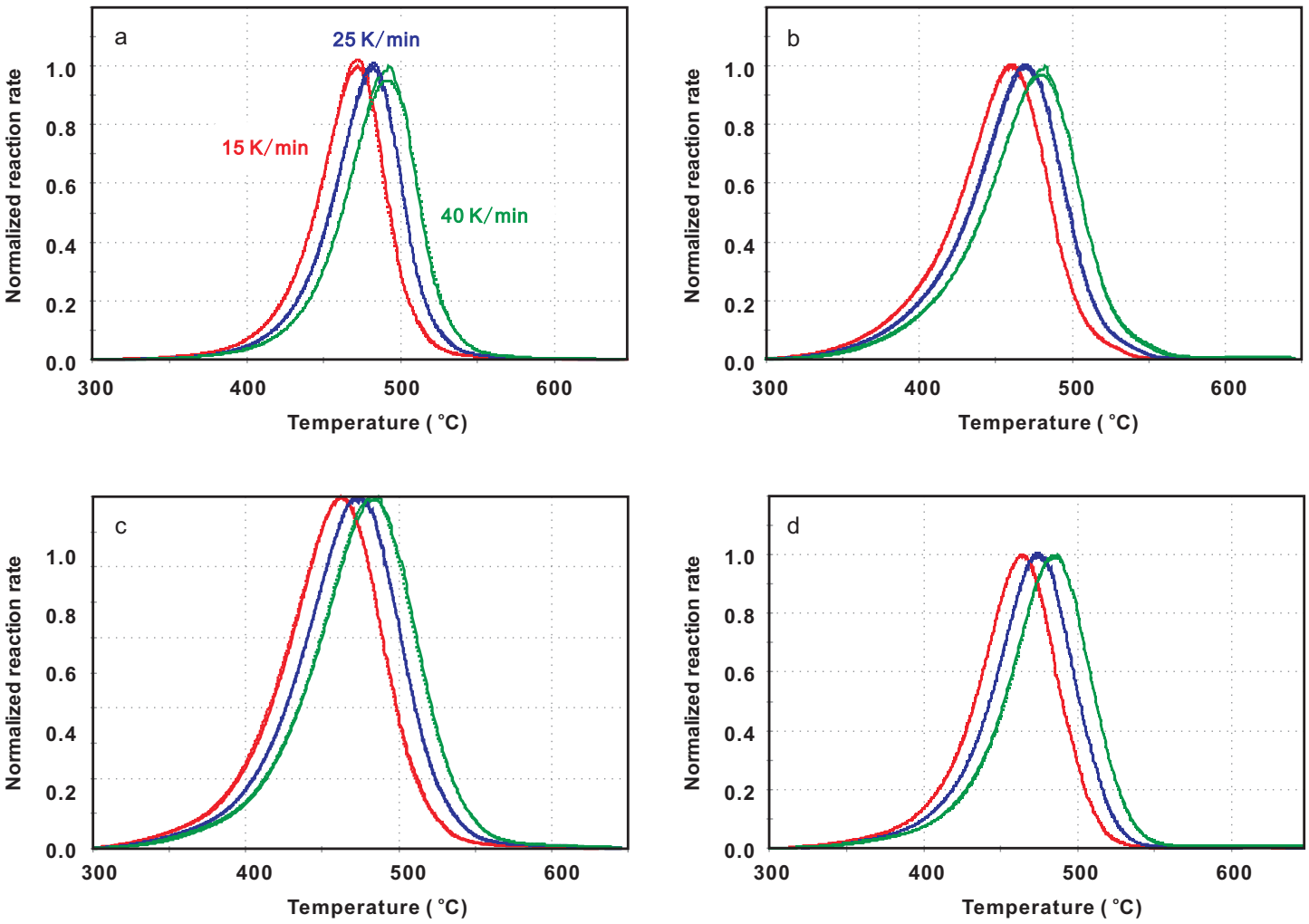

Fig. D2a Comparison of the measured data (symbols) and calculated or predicted hydrocarbon yield (curve) for heating rate group H. (with optimized A).
(a: Huadian; b: Maoming; c: Wang18; d: Ordos).

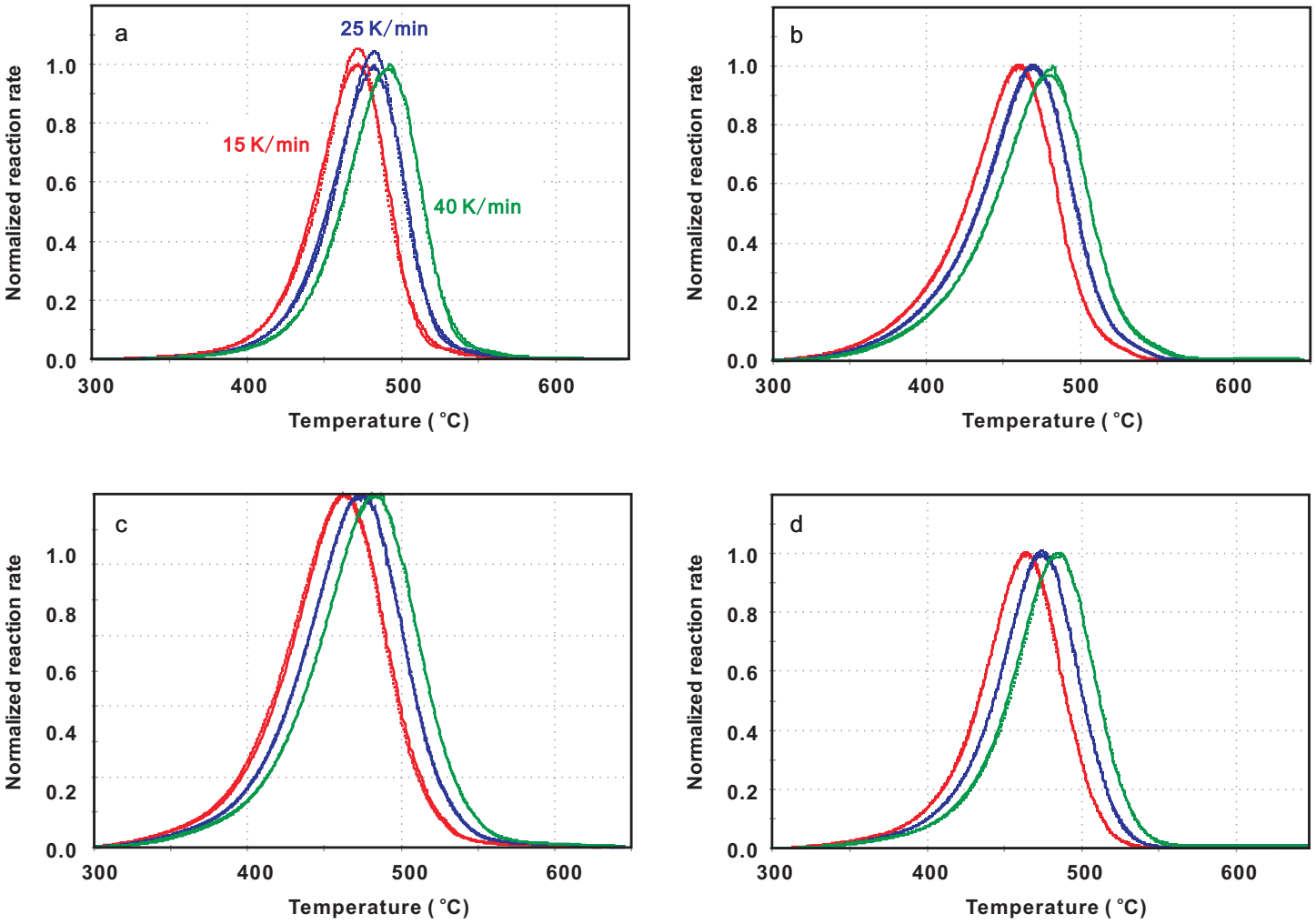

Fig. D2b Comparison of the measured data (symbols) and calculated or predicted hydrocarbon yield (curve) for heating rate group H. (with fixed A).
(a: Huadian; b: Maoming; c: Wang18; d: Ordos).

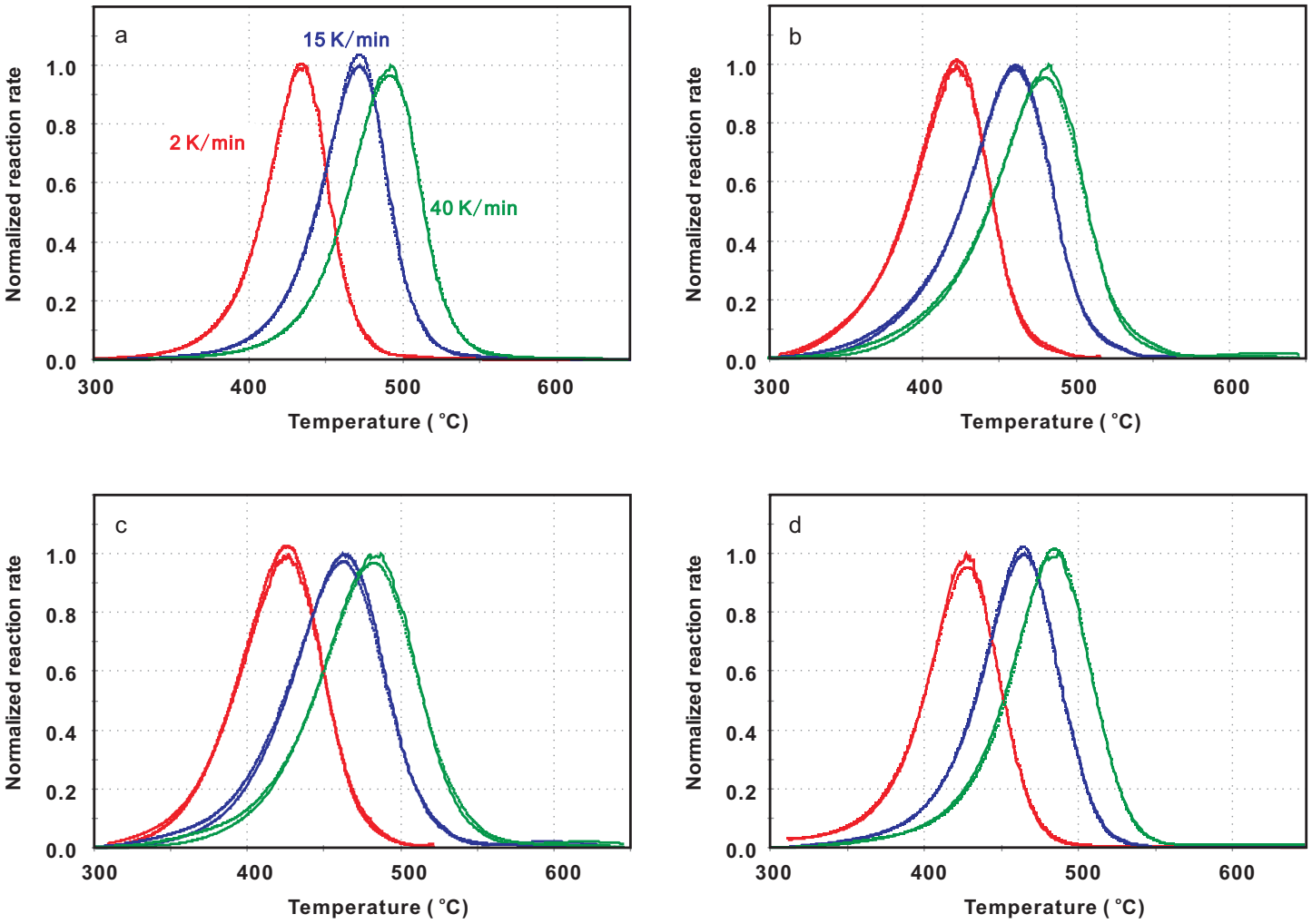

Fig. D3a Comparison of the measured data (symbols) and calculated or predicted hydrocarbon yield (curve) for heating rate group W_2. (with optimized A). (a: Huadian; b: Maoming; c: Wang18; d: Ordos).

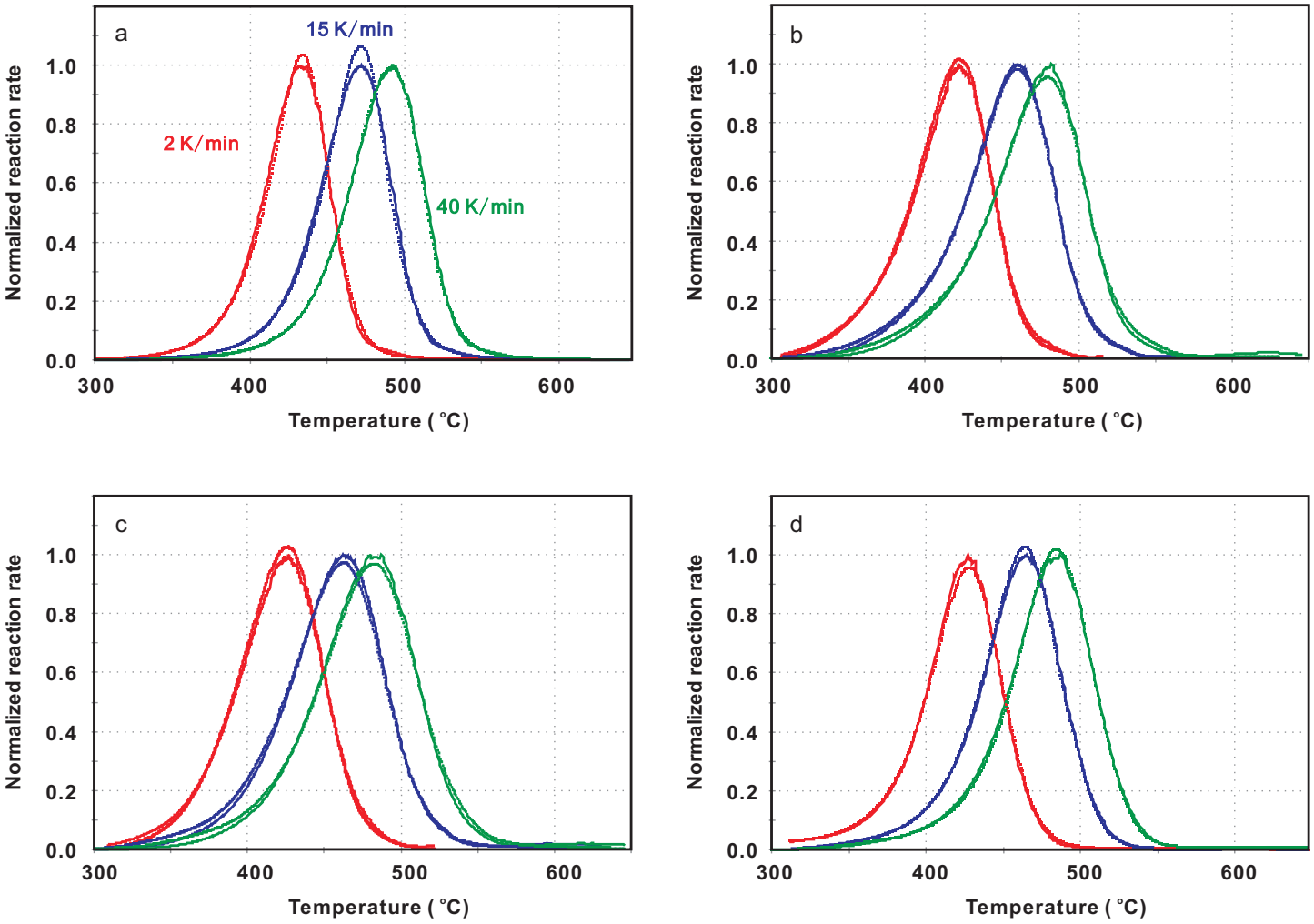

Fig. D3b Comparison of the measured data (symbols) and calculated or predicted hydrocarbon yield (curve) for heating rate group W_2. (with fixed A).
(a: Huadian; b: Maoming; c: Wang18; d: Ordos).

Table A1a Initial potential (Xi) and Ea with fixed A for heating group L

	Huadian	Maoming	Wang18	Ordos
A (sec^{-1})	3.00E+13			
Ea (kcal/mol)	(%)			
40				
41				
42				
43				0.13
44				0.33
45				0.30
46		1.09	0.67	1.22
47	0.94	2.07	0.05	0.13
48	0.58	1.93	2.49	2.50
49		6.54	4.82	1.70
50		0.96	5.43	
51		**27.86**	**20.19**	**19.49**
52	**39.72**	**36.60**	**27.53**	**37.67**
53	**53.30**	**19.03**	**27.98**	**22.01**
54			4.44	**11.50**
55	4.23	3.56	5.13	0.40
56	0.57	0.07	0.68	1.48
57				
58	0.20	0.29		
59			0.59	0.16
60				0.05
61				0.10
62	0.13			
63				0.39
64	0.32			
65				
66				
67				0.45
68				
69				
70				

Table A1b Initial potential (Xi) and Ea with fixed A for heating group H

	Huadian	Maoming	Wang18	Ordos
A (sec^{-1})	3.00E+13			
Ea (kcal/mol)	(%)			
40				
41				
42				
43		0.07	0.30	0.07
44	0.07	0.64	0.71	0.49
45		0.59	0.56	0.60
46	0.78	1.55	0.82	
47		2.53	1.63	1.93
48		2.21	1.81	1.10
49		5.63	5.33	
50		1.93	4.22	
51		**26.71**	**19.84**	**19.09**
52	**44.20**	**31.79**	**24.47**	**45.44**
53	**51.16**	**19.19**	**24.79**	**17.61**
54		0.50	6.06	**12.83**
55		5.47	7.61	
56	3.53	0.39		
57			0.97	0.40
58			0.24	
59				
60	0.25		0.30	
61		0.10	0.21	
62		0.69		0.45
63				
64			0.11	
65				
66				
67				
68				
69				
70				

Table A1c Initial potential (Xi) and Ea with fixed A for heating group W2

	Huadian	Maoming	Wang18	Ordos
A (sec^{-1})	3.00E+13			
Ea (kcal/mol)	(%)			
40				
41				
42				
43				0.21
44	0.09		0.06	0.30
45	0.05	0.68	0.74	0.53
46	0.28	1.19	0.17	0.72
47	0.75	2.13	1.29	0.53
48		2.53	1.89	2.46
49		4.79	4.68	
50		3.57	6.11	
51		**24.76**	**17.66**	**19.70**
52	**42.16**	**34.55**	**27.79**	**40.50**
53	**51.84**	**18.97**	**24.71**	**20.93**
54		0.06	6.72	**11.99**
55	1.99	4.92	4.82	
56	2.45		1.30	0.85
57				0.11
58				
59				
60	0.35	0.15	0.45	0.26
61	0.03	0.04	0.44	0.04
62		1.65		
63			1.18	
64				
65				0.88
66				
67				
68				
69				
70				

Table 1 Samples information

Locality	Lithology	Age	Top Depth (m)
Huadian	black oil shale	Tertiary	outcrop
Maoming	oil shale	E2-3y	outcrop
Wang18	oil shale	ES4	1628
Ordos	black mudstone	T3C7	outcrop

Table 2a TOC, Ro and Rock-Eval results from Wuxi

Sample	S1	S2	S3	Tmax	HI	OI	TOC	Ro
	mg/g sample			(°C)	mg/g TOC		(%)	(%)
Huadian	0.84	280.48	4.09	445	873	13	32.14	0.35
	0.78	278.55	4.31	442	867	13	32.13	
Maoming	0.57	38.10	2.14	432	537	30	7.10	0.37
	0.56	39.38	2.02	432	550	28	7.16	
Wang18	0.31	16.69	1.81	435	488	53	3.42	0.34
	0.29	17.05	1.72	437	510	51	3.34	
Ordos	1.23	37.22	4.23	436	348	39	10.71	0.43
	1.14	35.63	4.19	437	332	39	10.74	

Table 2b TOC and Rock-Eval results results from GFZ

Sample	S1	S2	S3	Tmax	HI	OI	TOC
	mg/g sample			(°C)	mg/g TOC		(%)
Huadian	0.55	160.11	4.19	447	503	13	31.80
	0.62	165.51	4.13	447	517	13	32.00
Maoming	0.23	33.20	2.05	431	468	29	7.10
	0.29	37.04	1.68	431	505	23	7.34
Wang18	0.14	13.95	2.23	426	389	62	3.59
	0.14	13.91	2.17	423	393	61	3.54
Ordos	0.91	43.13	5.92	434	308	42	14.00
	0.92	45.00	5.94	433	326	43	13.80

Table 3 Initial potential (Xi) &Ea with fixed A for heating group W_1 (wide heating rate range of 1, 15, 40K/min) from Wuxi (>10% of initial potential in bold). Results for heating groups L, H and W_2 are shown in Appendix A tables.

	Huadian	Maoming	Wang18	Ordos
A (sec^{-1})	3.00E+13			
Ea (kcal/mol)	(%)			
40				
41				
42				
43				0.03
44				0.41
45	0.05	0.05	0.55	0.36
46		1.61	0.15	0.95
47	1.25	1.28	1.35	0.20
48		2.96	1.62	2.86
49		4.97	5.28	
50		2.16	4.46	
51		**26.03**	**21.94**	**20.51**
52	**40.80**	**35.02**	**25.04**	**39.86**
53	**53.16**	**18.81**	**27.12**	**20.82**
54			3.14	**11.65**
55	2.76	4.58	5.95	
56	1.62		0.89	1.03
57				0.07
58				
59	0.10			
60		0.37	0.59	0.27
61	0.02		0.27	
62	0.25	2.17		
63			1.65	
64				
65				0.98
66				
67				
68				
69				
70				

Table 4a Initial potential (Xi) &Ea using optimized A of Huadian for Wuxi and GFZ results along with Wuxi pyrolysis results but using the GFZ optimized A in order to allow direct comparison of the Ea distributions.

	Huadian $W_1$1	Huadian $W_1$1 used GFZ A	Huadian GFZ
A (sec^{-1})	9.67E+13	4.20E+13	4.20E+13
Ea (kcal/mol)	(%)		
40			
41			
42			0.01
43			0.04
44			0.21
45		0.07	
46		0.19	0.75
47	0.36		
48	0.16	1.49	
49	0.47	0.15	3.41
50	1.58		
51			
52		5.15	
53		**81.08**	**72.53**
54	**74.18**		8.46
55	**10.43**	**11.05**	**13.17**
56	**11.53**		
57			
58		0.24	1.42
59	0.92	0.31	
60			
61			
62		0.14	
63	0.10	0.13	
64	0.28		
65			
66			
67			
68			
69			
70			

Table 4b Initial potential (Xi) &Ea using optimized A of Maoming for Wuxi and GFZ results along with Wuxi pyrolysis results but using the GFZ optimized A in order to allow direct comparison of the Ea distributions.

	Maoming $W_1$1	Maoming $W_1$1 used GFZ A	Maoming GFZ
A (sec^{-1})	1.63E+13	5.29E+13	5.29E+13
Ea (kcal/mol)	(%)		
40			
41			0.02
42			0.15
43			0.23
44			0.32
45	0.98		0.64
46	1.89	0.39	0.81
47	1.52	1.83	1.73
48	6.18	1.09	2.34
49		4.43	3.49
50	**22.33**	3.29	6.92
51	**36.91**	6.25	4.84
52	**22.80**	**29.62**	**26.16**
53		**32.26**	**25.82**
54	4.86	**13.93**	**17.99**
55	0.03	0.33	3.92
56		3.95	1.65
57			2.42
58			
59	0.31		
60			
61	2.20	0.40	0.55
62			
63		2.21	
64			
65			
66			
67			
68			
69			
70			

Table 4c Initial potential (Xi) &Ea using optimized A of Wang18 for Wuxi and GFZ results along with Wuxi pyrolysis results but using the GFZ optimized A in order to allow direct comparison of the Ea distributions.

	Wang18 $W_1$1	Wang18 W_1 used GFZ A	Wang18 GFZ
A (sec^{-1})	8.01E+12	2.63E+13	2.63E+13
Ea (kcal/mol)	(%)		
40			
41			0.06
42			0.18
43	0.20		0.21
44	0.37		0.57
45	0.90	0.63	0.49
46	0.85	0.25	1.05
47	5.30	1.17	1.01
48	2.27	2.67	3.66
49	**19.98**	4.33	3.51
50	**26.50**	7.24	**13.62**
51	**30.29**	**23.27**	**27.98**
52	4.66	**26.84**	**24.22**
53	5.38	**23.43**	**17.29**
54	1.12	1.67	1.91
55		6.00	3.33
56		0.21	0.13
57			0.43
58	0.32		0.17
59			0.03
60	1.85	0.53	
61			0.15
62		1.75	
63			
64			
65			
66			
67			
68			
69			
70			

Table 4d Initial potential (Xi) &Ea using optimized A of Ordos for Wuxi and GFZ results along with Wuxi pyrolysis results but using the GFZ optimized A in order to allow direct comparison of the Ea distributions.

	Ordos $W_1$1	Ordos $W_1$1 used GFZ A	Ordos GFZ
A (sec^{-1})	2.59E+13	5.83E+13	5.83E+13
Ea (kcal/mol)	(%)		
40			
41			
42			0.08
43	0.07		0.05
44	0.41	0.08	0.17
45	0.50	0.45	0.13
46	0.73	0.35	0.47
47	0.64	1.08	0.31
48	2.56		1.08
49		3.30	0.69
50			2.46
51	**29.99**		0.83
52	**34.65**	**24.16**	**18.94**
53	**20.66**	**35.55**	**30.28**
54	7.09	**21.12**	**21.64**
55	0.29	**10.60**	**14.82**
56	0.79	0.04	4.55
57		1.21	1.83
58			0.73
59			0.41
60	0.27	0.05	0.18
61	0.03		0.12
62		0.24	
63		0.10	0.23
64			
65			
66	1.32		
67		0.36	
68		0.03	
69			
70		1.29	

Table 5 Temperatures (°C) predicted for various transformation ratios at a geological heating rate of 1, 3, 10 K/Ma using the kinetics solutions for the **L**ow heating rate group and optimized A.

	TR	10%	30%	50%	70%	90%
Huadian	1K/Ma	135	145	150	154	162
	3K/Ma	142	152	156	161	169
	10K/Ma	149	159	164	169	177
Maoming	1K/Ma	108	122	128	134	142
	3K/Ma	115	129	135	141	149
	10K/Ma	122	136	143	149	157
Wang18	1K/Ma	102	114	120	126	131
	3K/Ma	108	121	127	134	143
	10K/Ma	116	128	135	142	151
Ordos	1K/Ma	117	130	136	142	151
	3K/Ma	124	137	143	149	159
	10 K/Ma	131	144	151	157	167

Table 6. Temperatures (°C) predicted for various transformation ratios at a geological heating rate of 3 K/Ma using the kinetics solutions at **L**ow, **H**igh and **W**ide heating rate ranges and A optimized from Wuxi and GFZ.

		TR	10%	30%	50%	70%	90%
Huadian	Wuxi	1, 2, 5 K/min	142	152	156	161	169
		15, 25, 40 K/min	140	149	154	158	166
		1, 15, 40 K/min	137	146	150	155	163
		2, 15, 40 K/min	137	146	151	155	163
	GFZ	0.7, 2, 5 K/min	133	143	148	152	161
Maoming	Wuxi	1, 2, 5 K/min	115	129	135	141	149
		15, 25, 40 K/min	114	131	138	144	154
		1, 15, 40 K/min	114	129	136	142	151
		2, 15, 40 K/min	113	128	135	141	150
	GFZ	0.7, 2, 5 K/min	114	133	141	148	159
Wang18	Wuxi	1, 2, 5 K/min	108	121	127	134	143
		15, 25, 40 K/min	105	120	128	135	145
		1, 15, 40 K/min	114	127	134	141	152
		2, 15, 40 K/min	118	132	139	146	157

	GFZ	0.7, 2, 5 K/min	115	129	136	143	154
Ordos	Wuxi	1, 2, 5 K/min	124	137	143	149	159
		15, 25, 40 K/min	120	130	136	141	150
		1, 15, 40 K/min	124	135	141	147	156
		2, 15, 40 K/min	126	138	143	150	159
	GFZ	0.7, 2, 5 K/min	128	140	146	153	165

Fig. 1. Location of four organic rich samples from China.

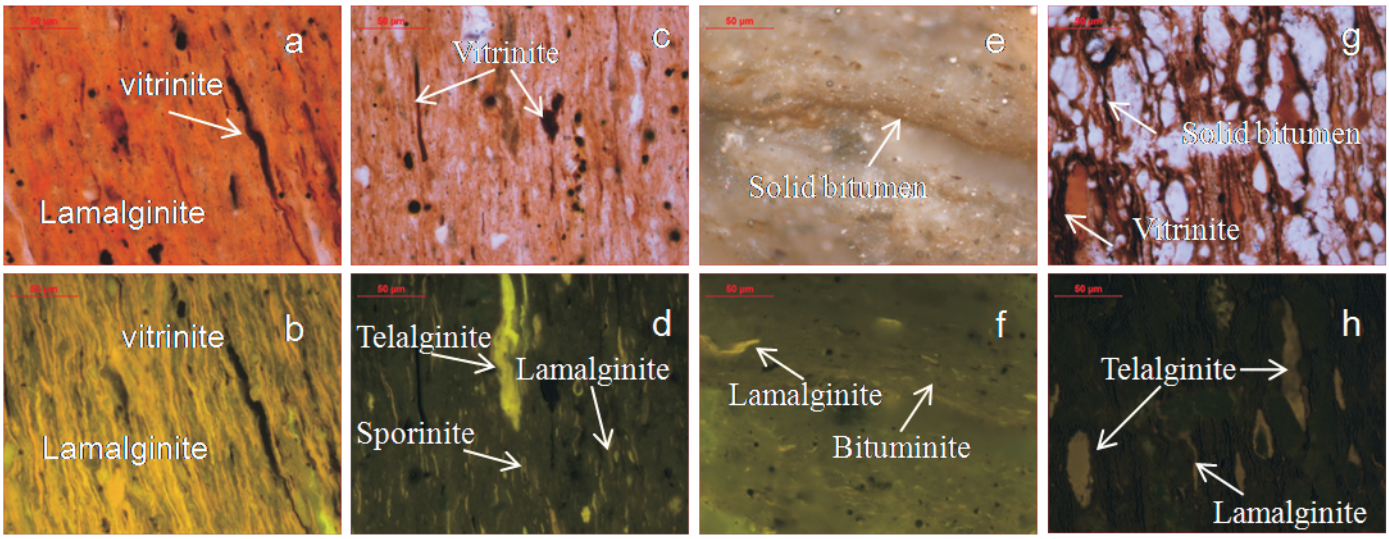

Fig. 2. Photomicrographs of macerals in the four samples (a, c, g: transmitted light; e: reflected white light; b, d, f, h: fluorescene blue light). (a, b:Huadian; c, d: Maoming; e, f: Wang18; g, h: Ordos), polished thin section, immersion oil objective, ×500, scale bar = 50 μm.

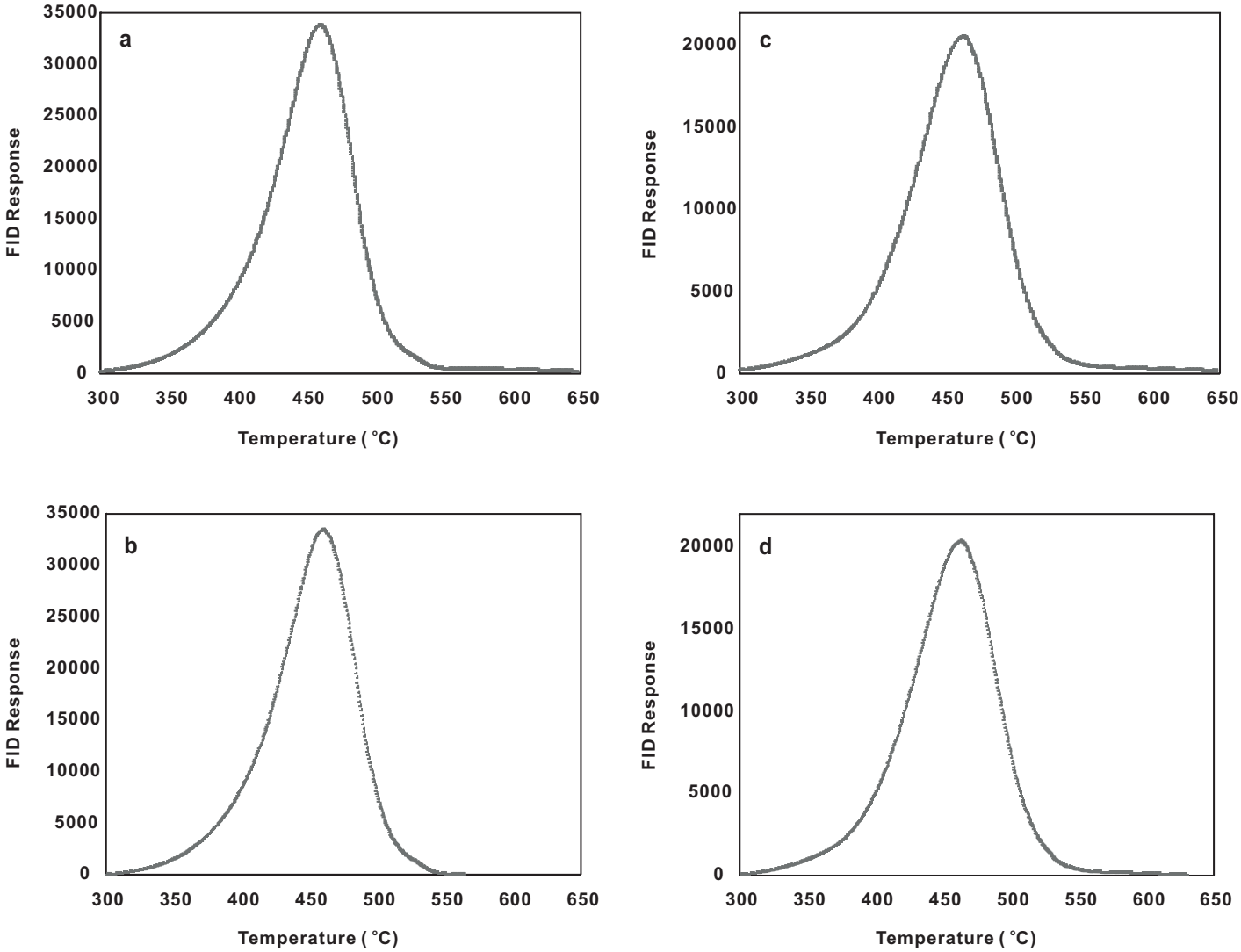

Fig. 3. Examples of RE6 pyrolysis traces at 15 K/min. (a: excluding the S1 peak and the cool down signal for the Maoming sample; b: traces after signal has been trimmed, thinned and the baseline corrected for the Maoming sample; c: excluding the S1 peak and the cool down signal for the Wang18 sample; d: traces after signal has been trimmed, thinned and the baseline corrected for the Wang18 sample).

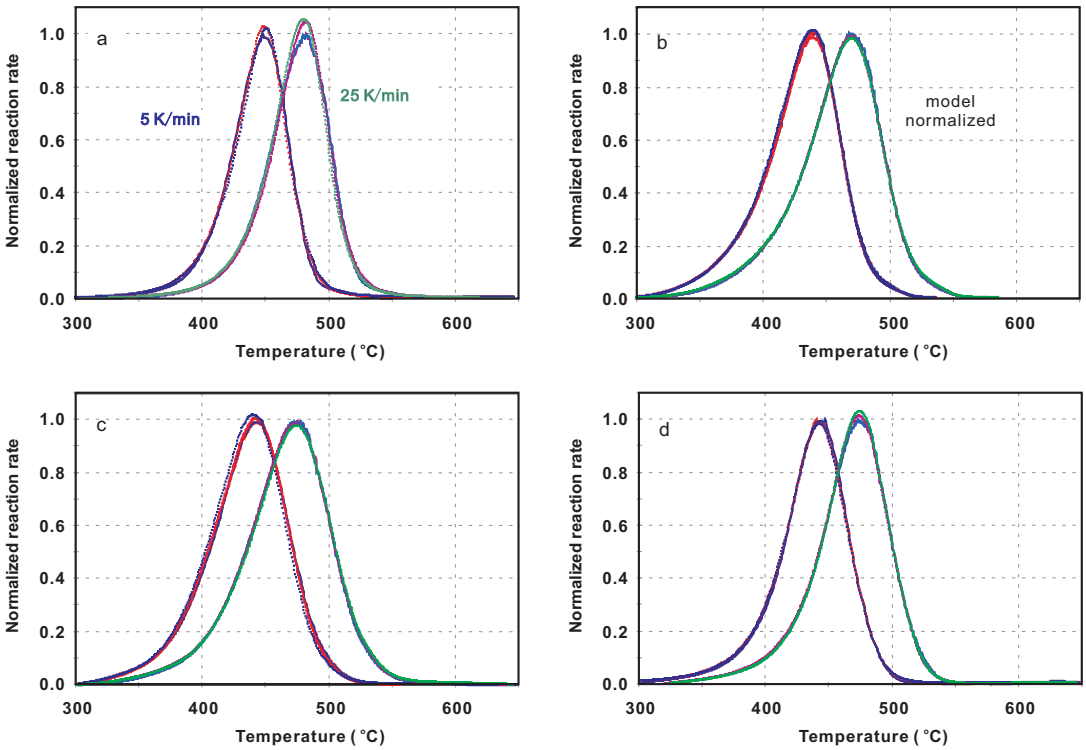

Fig. 4. A comparison of replicate RE6 runs at 5 K/min and 25 K/min (a) with optimized A and (b) with fixed A. (Two sets of measured data and two models are shown for each sample and each heating rate. Traces normalized to the measured data instead of the model. a: Huadian; b: Maoming; c: Wang18; d: Ordos). Resulting optimized kinetics solutions calculated using one or the other of the replicate data sets similarly provided essentially identical results.

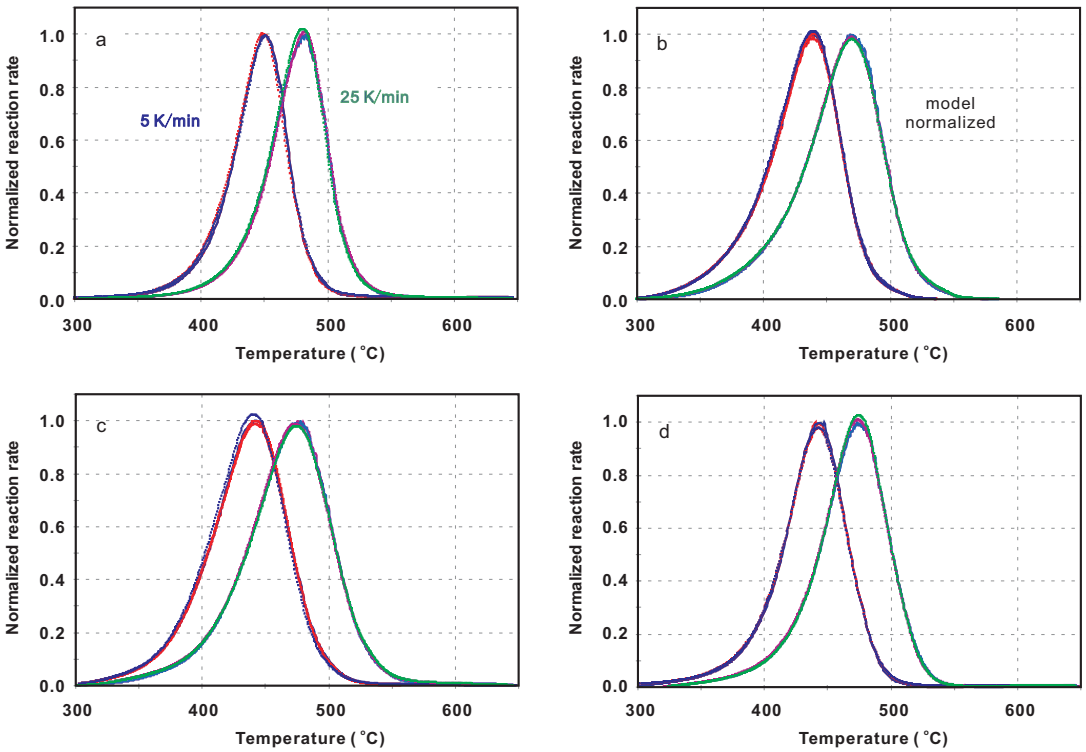

Fig. 4b. A comparison of replicate RE6 runs at 5 K/min and 25 K/min and models calculated with fixed A =3×10^{13}/s. (a: Huadian; b: Maoming; c: Wang18; d: Ordos).

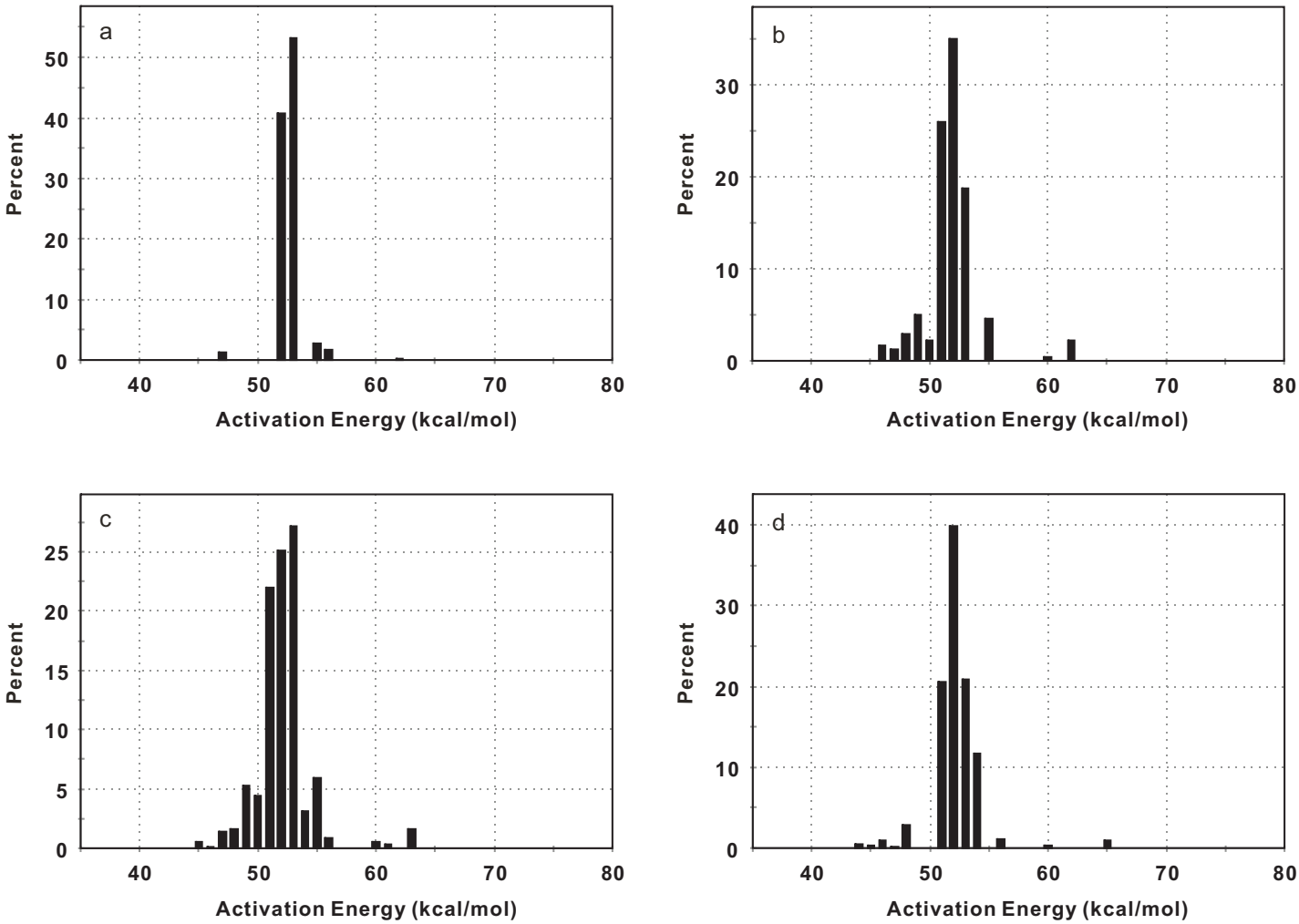

Fig. 5. Initial potential (X_i) histograms for fixed A (3×10^{13}/s) solutions for group W_1 heating rates. (W_1: 1, 15, 40 K/min; a: Huadian; b: Maoming; c: Wang18; d: Ordos).

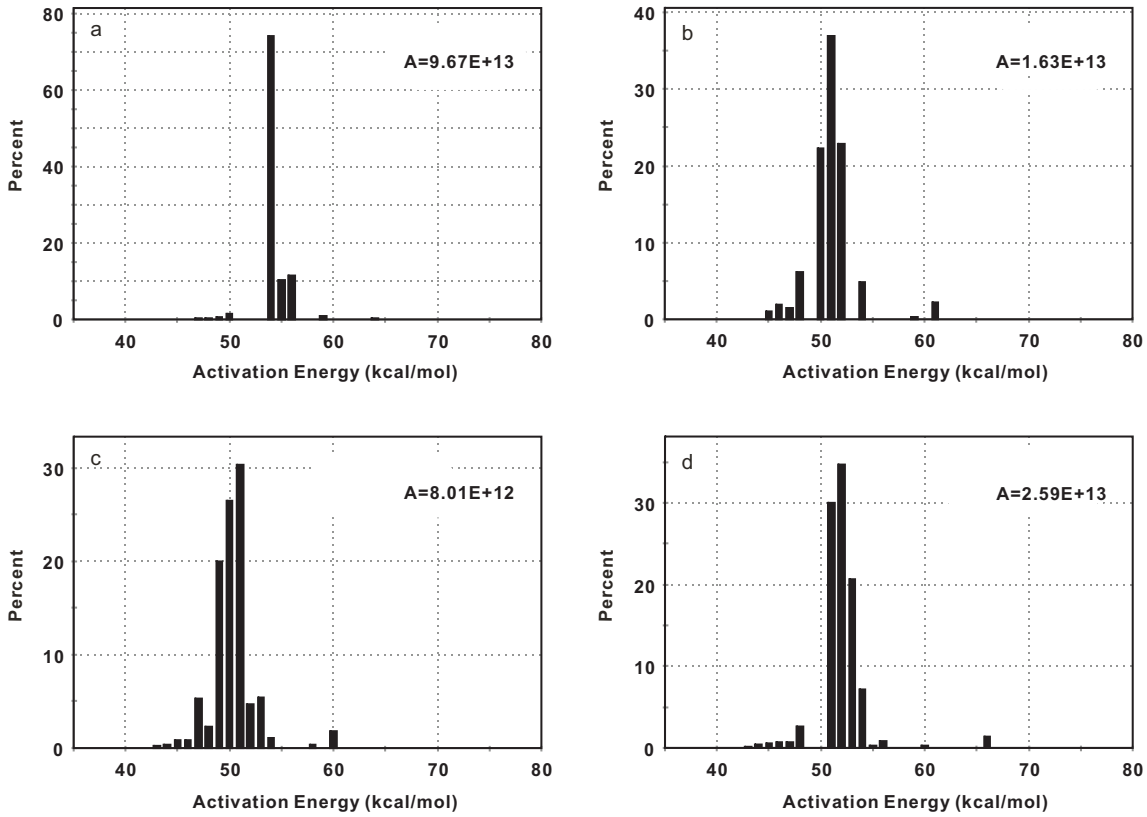

Fig. 6a. Initial potential (X_i) and activation energy distributions calculated for each sample with the frequency factor (A) optimized at group W_1 by Re6.(a: Huadian; b: Maoming; c: Wang18; d: Ordos).

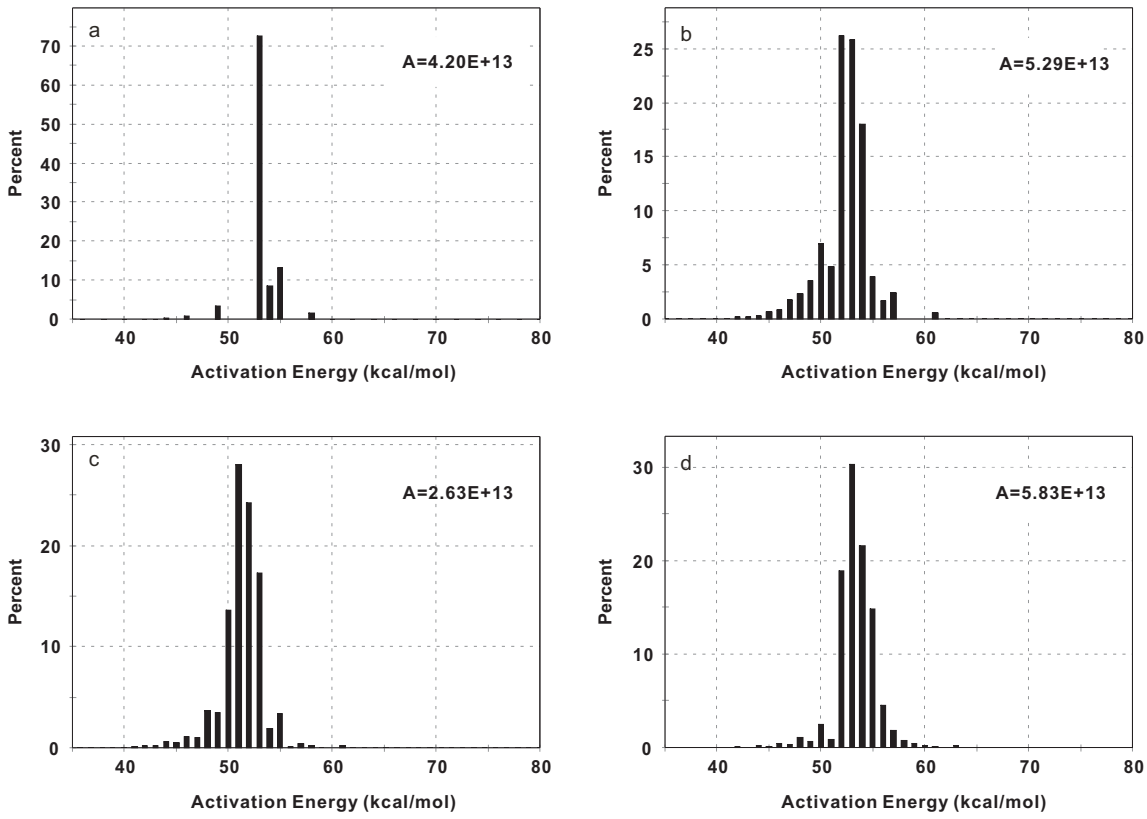

Fig. 6b. Initial potential (X_i) and activation energy distributions calculated for each sample with the frequency factor (A) optimized by SRA. (a: Huadian; b: Maoming; c: Wang18; d: Ordos).

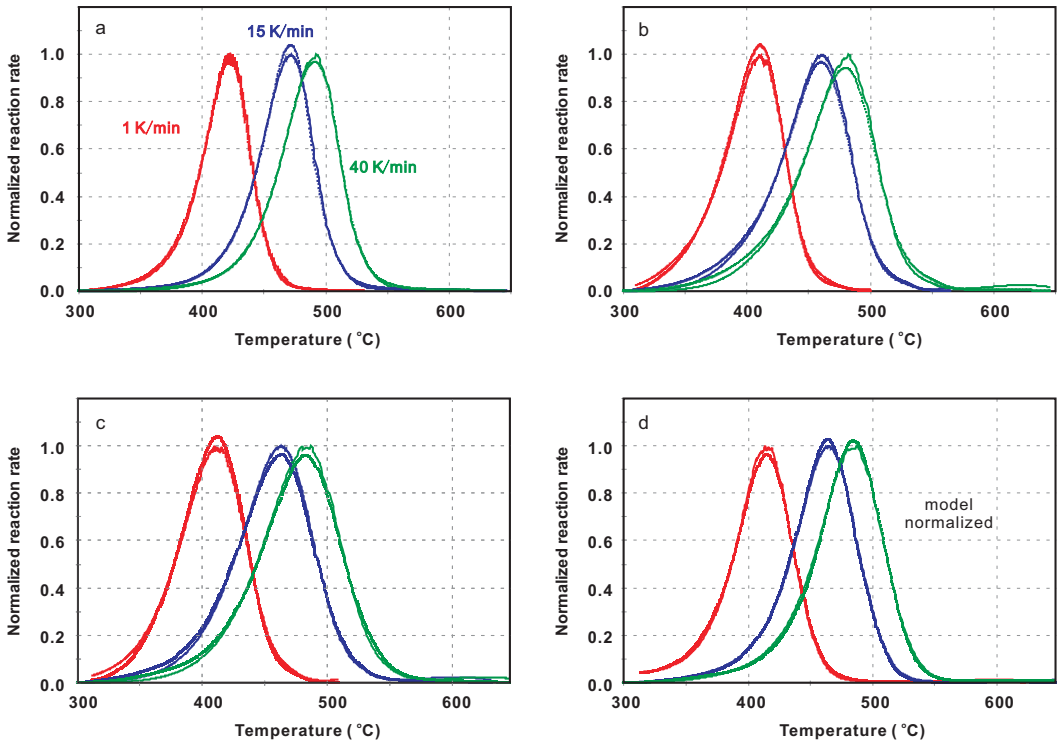

Fig. 7a. Comparison of the measured data (symbols) and calculated or predicted hydrocarbon yield (curve) for heating rate group W_1. (W_1: 1, 15 and 40 K/min; a: Huadian; b: Maoming; c: Wang18; d: Ordos). (with optimized A).

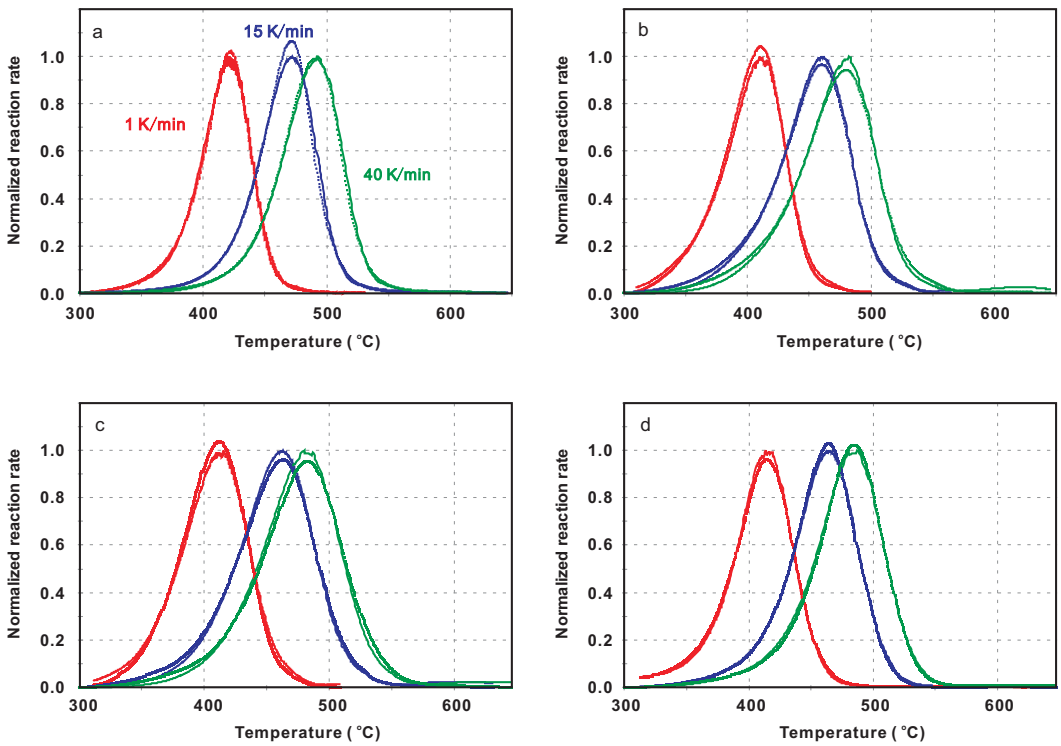

Fig. 7b. Comparison of the measured data (symbols) and calculated or predicted hydrocarbon yield (curve) for heating rate group W_1 .(W_1: 1, 15 and 40 K/min; a: Huadian; b: Maoming; c: Wang18; d: Ordos). (with fixed A).

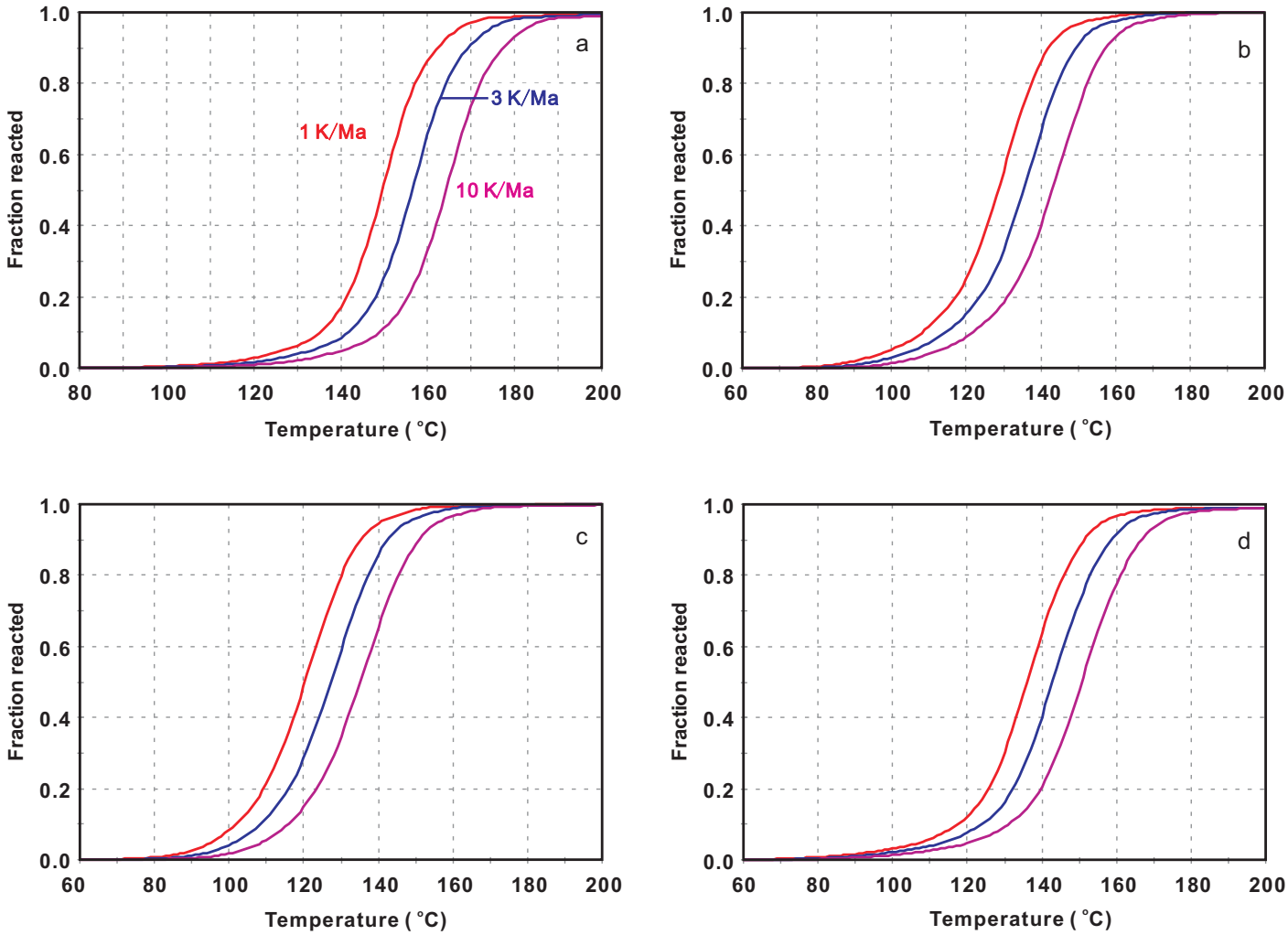

Fig. 8. Comparison of the calculated cumulative HC generation at geological heating rates of 1, 3 and 10 K/Ma for kinetics solutions derived for the low heating rate group L. (L: 1, 2 and 5 K/min) and A optimized for (a) Huadian (b) Maoming (c)Wang18 (d) Ordos

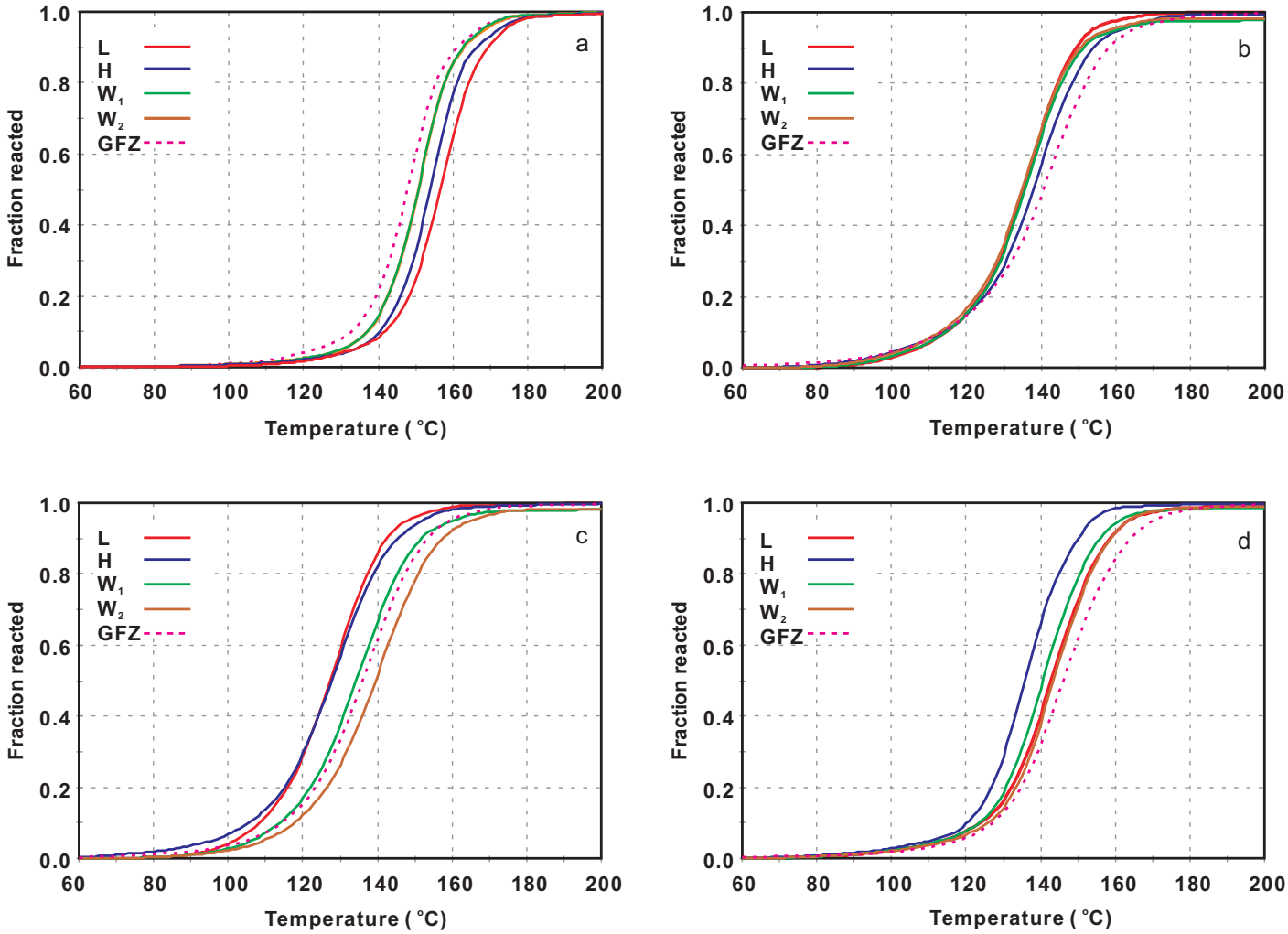

Fig. 9. A comparison of the predicted cumulative hydrocarbon generation at 3 K/Ma for each of the samples and for each of the heating rates groups from the two labs. (L: 1, 2 and 5 K/min; H: 15, 25 and 40 K/min; W_1: 1, 15 and 40 K/min; W_2:2, 15 and 40 K/min and 0.7, 2.0 and 5.0 K/min for GFZ. a: Huadian; b: Maoming; c: Wang18; d: Ordos)

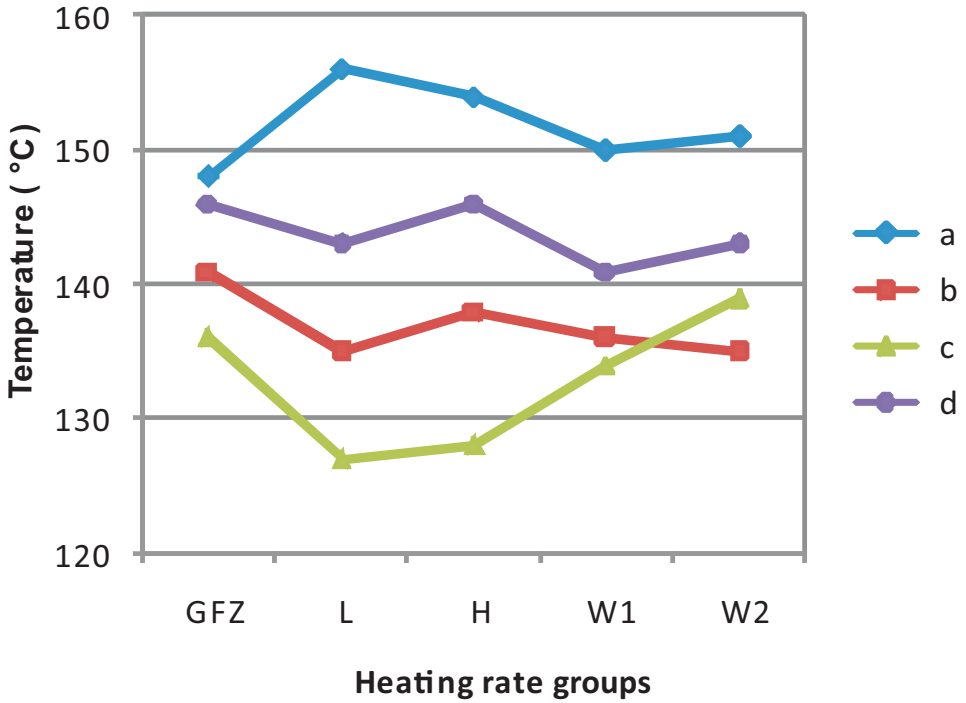

Fig. 10. Temperatures predicted for 50% TR of samples heated at 3 K/Ma as a function of the heating rates used to optimize a kinetics solution. (a: Huadian; b: Maoming; c: Wang18; d: Ordos).Peters et al. (2015) have indicated that solutions Wide1 or Wide2 should provide the best models because these have heating rates that differ by 40× and 20×, respectively. The GFZ-low solution has the lowest heating rate range (0.7–5 K/min) but only a 7.1×ratio. The Low heating rates (Wuxi: 1, 2 and 5 K/min) have a slightly lower ratio of 5, but significantly lower predicted 50% TR temperature for three of the samples.